DIRAC POINTS FOR SQUARE LATTICE PHOTONIC CRYSTALS

CHIU-YEN KAO*, JUNSHAN LIN†, AND BRAXTON OSTING‡

Abstract. This work is concerned with Dirac points in dispersion surfaces associated with the wave equation where the material coefficient attains the translational symmetries of a square lattice. It is proved in Keller et. al. (2018) that the spectrum of the Schrödinger operator over a square lattice does not have a Dirac point at the high symmetry point of the Brillouin zone, at least for the lower bands. In the high-contrast limit, we prove the existence of the Dirac point for the 2D Helmholtz operator over a square lattice away from the high symmetry point of the Brillouin zone, if the dielectric function of the periodic medium attains reflection symmetry. In particular, the two-dimensional eigenspace at the Dirac point is spanned by eigenfunctions with the opposite parity. Based on this observation, we propose a computational inverse design method using the local-density-of-state to generate a Dirac point at the desired Bloch wave vector and frequency. Numerous numerical results demonstrate the capability of our algorithm to generate a desired Dirac point robustly.

Key words. Square lattice, Dirac point, Helmholtz equation, eigenvalue problem, inverse design.

AMS subject classifications. 35B10, 35C20, 35P05, 35J05, 35Q93, 65K10, 65N25.

1. Introduction.

A Dirac point is formed by the conical intersection of two dispersion surfaces in the spectral bands of a periodic operator. Mathematically, it is a degenerate point $(\boldsymbol{\kappa}^*, \omega^*)$ in the spectrum such that two dispersion surfaces forming the degenerate point have the expansion

$$\omega^{\pm}(\boldsymbol{\kappa}) = \omega^* + \alpha_{\pm}\left(\frac{\boldsymbol{\kappa}-\boldsymbol{\kappa}^*}{|\boldsymbol{\kappa}-\boldsymbol{\kappa}^*|}\right)\cdot|\boldsymbol{\kappa}-\boldsymbol{\kappa}^*| + O(|\boldsymbol{\kappa}-\boldsymbol{\kappa}^*|^2) \tag{1.1}$$

with nonzero slope functions, $\alpha_{\pm}\left(\frac{\boldsymbol{\kappa}-\boldsymbol{\kappa}^*}{|\boldsymbol{\kappa}-\boldsymbol{\kappa}^*|}\right)$. Dirac points play a special role in the study of topological materials, which attain unique wave transport property induced by the topology of the material [12, 27]. In general, for a photonic/phononic material exhibiting a Dirac point in the spectrum, a spectral band gap can be opened near the Dirac point either by breaking the time-reversal symmetry or the space-inversion symmetry to create nontrivial topological phases [6, 9, 21, 24, 25, 33]. From this point of view, a Dirac point can be viewed as a transition point for materials with different topological phases.

The mathematical analysis of Dirac points dates back to the study of the tight-binding approximation model for graphene in [30, 32]. Due to the increasing interest in topological insulators in recent years, Dirac points were investigated for a broad class of partial differential operators over the honeycomb lattices. More specifically, Dirac points for the Schrödinger equation model of graphene were considered in [10] over the honeycomb lattice with a weak potential and later thoroughly studied in [7] for potentials that are not necessarily weak. An alternative approach based on the symmetry argument was presented in [4] for the analysis of Dirac points over graphene. These results are then generalized to elliptic operators with other settings over the

*Department of Mathematical Sciences, Claremont McKenna College, Claremont, CA. (ckao@cmc.edu) This author was partially supported by NSF grant DMS-2208373.

†Department of Mathematics and Statistics, Auburn University, Auburn, AL 36849 (jzl0097@auburn.edu). This author was partially supported by NSF grant DMS-2410645.

‡Department of Mathematics, University of Utah, Salt Lake City, UT (osting@math.utah.edu). This author acknowledges partial support from NSF DMS-2136198.

honeycomb lattice, including point scatterers, high-contrast medium, impenetrable obstacles, resonant bubbles, etc [2, 5, 8, 18, 22].

The Dirac point in the honeycomb lattice occurs at the high symmetry points of the Brillouin zone. Its existence is attributed to the special symmetry that is imposed for the medium coefficients of the differential operator. For instance, the Schrödinger operator with a potential function that is inversion symmetric and invariant under a $\frac{2\pi}{3}$-rotation in the periodic cell allows the decomposition of the solution space $\mathcal{H}$ into three subspaces $\mathcal{H}_0 \oplus \mathcal{H}_1 \oplus \mathcal{H}_2$, wherein a function $\phi \in \mathcal{H}_j$ gains a phase of $e^{\imath j 2\pi/3}$ if rotated by $\frac{2\pi}{3}$ in the spatial domain. At the Dirac point, the two-dimensional eigenspace is spanned by $\phi_1 \in \mathcal{H}_1$ and $\phi_2 \in \mathcal{H}_2$ with the relation $\phi_2(\mathbf{x}) = \overline{\phi_1(-\mathbf{x})}$. The slope of the Dirac cone is nontrivial because of the different rotational behavior of the eigenfunctions $\phi_1(\mathbf{x})$ and $\phi_2(\mathbf{x})$ in two subspaces $\mathcal{H}_1$ and $\mathcal{H}_2$.

For the reasons mentioned above, the majority of the study for the Dirac point is carried out over the honeycomb lattice. The Dirac point in other lattices is much less investigated due to the lack of the desired symmetry to generate a non-trivial slope value for the dispersion surfaces at the degeneracy. In this work, we aim to study the Dirac point in the square lattice. It is proven in [14] that, very different from the honeycomb lattice, the Schrödinger operator over a square lattice does not exhibit a Dirac point at the high symmetry point of the Brillouin zone, at least for the first five spectral bands. We aim to prove the existence of the Dirac point for Bloch wave vectors away from the high-symmetry point in the Brillouin zone, if the partial differential operator attains reflection symmetry in space. Furthermore, we propose an inverse design method to generate a Dirac point at the desired Bloch wavenumber and frequency. Using this method, we demonstrate that a Dirac point can be generated at many locations in the Brillouin zone.

1.1. Main contribution of this work. We consider the square lattice in $\mathbb{R}^2$ given by $\Lambda := \mathbb{Z}\mathbf{e}_1 \oplus \mathbb{Z}\mathbf{e}_2 := \{\ell_1\mathbf{e}_1 + \ell_2\mathbf{e}_2 \colon \ell_1, \ell_2 \in \mathbb{Z}\}$, where $\mathbf{e}_1 = a(1,0)$ and $\mathbf{e}_2 = a(0,1)$ are the lattice vectors and a is the lattice constant. The dielectric function $\rho(\mathbf{x})$ is a periodic in $\mathbb{R}^2$ with $\rho(\mathbf{x}+\mathbf{e}) = \rho(\mathbf{x})$ for any $\mathbf{e} \in \Lambda$. Let $\boldsymbol{\kappa}_1$ and $\boldsymbol{\kappa}_2$ be the reciprocal lattice vectors that satisfy $\mathbf{e}_i \cdot \boldsymbol{\kappa}_j = 2\pi\delta_{ij}$ for $i,j = 1,2$. We define the reciprocal lattice $\Lambda^* = \mathbb{Z}\boldsymbol{\kappa}_1 \oplus \mathbb{Z}\boldsymbol{\kappa}_2 := \{\ell_1\boldsymbol{\kappa}_1 + \ell_2\boldsymbol{\kappa}_2 \colon \ell_1, \ell_2 \in \mathbb{Z}\}$, and denote the fundamental cell in Λ^*, or the Brillouin zone, by $\mathcal{B}$. Define $\Gamma = (0,0)$, $X = (\pi/a, 0)$ and $M = (\pi/a, \pi/a)$, then the triangle formed by the vertices $\Gamma X M$ is called the reduced Brillouin zone when photonic crystals have rotation and reflection (with respect to x_1-axis and x_2-axis) symmetry.

Let $Y := \{t_1\mathbf{e}_1 + t_2\mathbf{e}_2 \,|\, 0 \le t_1, t_2 \le 1\}$ be the fundamental cell of the lattice. For each Bloch wave vector $\boldsymbol{\kappa} \in \mathcal{B}$, we consider the following eigenvalue problem with the frequency $\omega \in \mathbb{R}$:

$$\Delta\psi(\boldsymbol{\kappa},\omega;\mathbf{x}) + \omega^2\rho(\mathbf{x})\psi(\boldsymbol{\kappa},\omega;\mathbf{x}) = 0, \qquad \mathbf{x} \in Y + \Lambda, \tag{1.2a}$$

$$\psi(\boldsymbol{\kappa},\omega;\mathbf{x}+\mathbf{e}) = e^{\imath\boldsymbol{\kappa}\cdot\mathbf{e}}\psi(\boldsymbol{\kappa},\omega;\mathbf{x}), \qquad \text{for } \mathbf{e} \in \Lambda. \tag{1.2b}$$

The eigenfunction ψ is called the Bloch mode, which can be written as $\psi(\boldsymbol{\kappa},\omega;\mathbf{x}) = e^{\imath\boldsymbol{\kappa}\cdot\mathbf{x}}\phi(\boldsymbol{\kappa},\omega;\mathbf{x})$, wherein ϕ is a periodic function satisfying $\phi(\boldsymbol{\kappa},\omega;\mathbf{x}+\mathbf{e}) = \phi(\boldsymbol{\kappa},\omega;\mathbf{x})$ for all $\mathbf{e} \in \Lambda$.

We first consider the special configuration when the periodic medium consists of periodically arranged impenetrable inclusions (e.g., perfect conductors) embedded in a homogeneous background medium. In such a scenario, the PDE (1.2a) reduces to

$$\Delta\psi(\boldsymbol{\kappa},\omega;\mathbf{x}) + \omega^2\psi(\boldsymbol{\kappa},\omega;\mathbf{x}) = 0, \quad \mathbf{x} \in (Y\backslash D_\varepsilon) + \Lambda, \tag{1.3a}$$

where D_ε denotes the impenetrable inclusion in the fundamental cell Y with size ε. Along the boundary of the inclusions, the Dirichlet boundary condition

$$\psi(\boldsymbol{\kappa}, \omega; \mathbf{x}) = 0, \quad \mathbf{x} \in \partial D_\varepsilon + \Lambda \tag{1.3b}$$

is imposed. Our first goal is to prove the existence of the Dirac point for certain $\boldsymbol{\kappa}$ on the boundary of the reduced Brillouin zone $\Gamma X M$ if D_ε is a disk with radius ε that is centered at $\mathbf{x}_c = \frac{1}{2}(\mathbf{e}_1 + \mathbf{e}_2)$. Furthermore, we show that the eigenspace at the Dirac point is spanned by two Bloch modes with opposite parity. The existence of Dirac points in the lower bands are summarized in Theorems 3.15, 4.1, and 4.2 for some $\boldsymbol{\kappa}^*$ on ΓX, ΓM and XM respectively. We apply the integral equation approach for solving the eigenvalue problem (1.3a) and perform the spectral analysis of the Laplacian operator $-\Delta$ via the characteristic value of the underlying integral operator.

Our second goal is to investigate the existence of Dirac points for $\boldsymbol{\kappa}$ not necessarily covered in the theoretical analysis. To this end, we consider the inverse design problem of solving the medium coefficient $\rho(\mathbf{x})$ such that the eigenvalue problem (1.2a) attains a Dirac point at the desired pair $(\boldsymbol{\kappa}^*, \omega^*)$. Note that a brute-force optimization framework of minimizing the distance between two frequency bands at $\boldsymbol{\kappa}^*$ while enforcing the constraint of nonzero slope value α in (1.1) may not have solutions. From the quantitative spectral analysis, it is observed that the parity of two independent eigenfunctions is opposite at the Dirac point. Therefore, we impose the constraint on the parity of eigenfunctions, instead of eigenvalues directly, to create a Dirac point. The desired parity for the eigenfunctions can be realized by optimizing the so-called the local density-of-state method (LDOS) [19]. The proposed computational inverse design framework is able to produce a Dirac point at the desired location $(\boldsymbol{\kappa}^*, \omega^*)$. For instance, in Figure 5.2, we show that a material coefficient can be constructed so that the second and third spectral bands exhibit a Dirac point at locations along the XM interval in the Brillouin zone.

The rest of the paper is organized as follows. In Section 2, we reformulate the eigenvalue problem (1.3) as an equivalent integral equation. Section 3 and 4 examine the existence of Dirac points for (1.3) on the boundary of the reduced Brillouin zone by analyzing the characteristic values of the integral operator. In Section 5, we present the inverse design approach and various numerical examples to demonstrate the effectiveness of the approach.

2. Integral equation formulation for the eigenvalue problem (1.3). For a given Bloch wave vector $\boldsymbol{\kappa} \in \mathcal{B}$ and frequency $\omega \in \mathbb{R}$, we use $G(\boldsymbol{\kappa}, \omega; \mathbf{x})$ to denote the corresponding quasi-periodic Green's function that satisfies

$$(\Delta + \omega^2) G(\boldsymbol{\kappa}, \omega; \mathbf{x}) = \sum_{\mathbf{e} \in \Lambda} e^{\imath \boldsymbol{\kappa} \cdot \mathbf{e}} \delta(\mathbf{x} - \mathbf{e}) \quad \text{for } \mathbf{x} \in \mathbb{R}^2. \tag{2.1}$$

It can be shown that

$$G(\boldsymbol{\kappa}, \omega; \mathbf{x}) = -\frac{\imath}{4} \sum_{\mathbf{e} \in \Lambda} e^{\imath \boldsymbol{\kappa} \cdot \mathbf{e}} H_0^{(1)}(\omega |\mathbf{x} - \mathbf{e}|), \tag{2.2}$$

where $H_0^{(1)}$ is the zeroth-order Hankel function of the first kind. Alternatively, $G(\boldsymbol{\kappa}, \omega; \mathbf{x})$ adopts the following spectral representation (cf. [1, 3]):

$$G(\boldsymbol{\kappa}, \omega; \mathbf{x}) = \frac{1}{|Y|} \sum_{\mathbf{q} \in \Lambda^*} \frac{e^{\imath (\boldsymbol{\kappa} + \mathbf{q}) \cdot \mathbf{x}}}{\omega^2 - |\boldsymbol{\kappa} + \mathbf{q}|^2}. \tag{2.3}$$

Note the Green's function is not well defined when the frequency satisfies $|\omega| = |\boldsymbol{\kappa}+\mathbf{q}|$ for some $\mathbf{q} \in \Lambda^*$. We call such a frequency a singular frequency and denote the set of singular frequencies by

$$\Omega_{\text{sing}}(\boldsymbol{\kappa}) := \{\omega \colon |\omega| = |\boldsymbol{\kappa} + \mathbf{q}| \text{ for some } \mathbf{q} \in \Lambda^*\}.$$

For each $\boldsymbol{\kappa} \in \mathcal{B}$, we arrange all the singular frequencies in $\Omega_{\text{sing}}(\boldsymbol{\kappa})$ in ascending order and denote them as $\bar{\omega}_1(\boldsymbol{\kappa}) \le \bar{\omega}_2(\boldsymbol{\kappa}) \le \cdots \le \bar{\omega}_n(\boldsymbol{\kappa}) \le \bar{\omega}_{n+1}(\boldsymbol{\kappa}) \le \cdots$.

We now introduce the following single-layer potential

$$[\mathcal{S}^{\boldsymbol{\kappa},\omega}\varphi](\mathbf{x}) := \int_{\mathbf{y}\in\partial D_\varepsilon} G(\boldsymbol{\kappa},\omega;\mathbf{x}-\mathbf{y})\varphi(\mathbf{y})\, ds_{\mathbf{y}}, \quad \mathbf{x} \in (Y\backslash D_\varepsilon) + \Lambda, \tag{2.4}$$

where φ is a density function on ∂D_ε. Let $\mathcal{H}^s(\partial D_\varepsilon)$ be the standard Sobolev space of order s over the boundary of D_ε, i.e.,

$$\mathcal{H}^s(\partial D_\varepsilon) := \Big\{ f \in L^2(\partial D_\varepsilon) \colon |\sum_{n\in\mathbb{Z}} (1+|n|^2)^s |\hat{f}_n|^2 < \infty \text{ where } \hat{f}_n \text{ are its Fourier coefficients} \Big\}.$$

It is well-known that $\mathcal{S}^{\boldsymbol{\kappa},\omega}$ is bounded from $\mathcal{H}^{-1/2}(\partial D_\varepsilon)$ to $\mathcal{H}^{1/2}(\partial D_\varepsilon)$ [1, 3]. We represent the Bloch mode for the eigenvalue problem (1.3) using the above defined layer potential by $\psi = \mathcal{S}^{\boldsymbol{\kappa},\omega}\varphi$. Using the Green's identity, it is easy to check that (ω, ψ) is an eigenpair for the Dirichlet problem (1.3) if and only if there exists a density function $\varphi \in \mathcal{H}^{-1/2}(\partial D_\varepsilon)$ such that

$$[\mathcal{S}^{\boldsymbol{\kappa},\omega}\varphi](\mathbf{x}) = 0 \quad \text{for } \mathbf{x} \in \partial D_\varepsilon. \tag{2.5}$$

To facilitate the asymptotic analysis, we apply the change of variables to rewrite the above integral equation as

$$[\mathcal{S}_\varepsilon^{\boldsymbol{\kappa},\omega}\varphi](\mathbf{x}) = 0 \quad \text{for } \mathbf{x} \in \partial D_1, \tag{2.6}$$

where the integral operator $\mathcal{S}_\varepsilon^{\boldsymbol{\kappa},\omega}$ takes the form

$$[\mathcal{S}_\varepsilon^{\boldsymbol{\kappa},\omega}\varphi](\mathbf{x}) := \int_{\mathbf{y}\in\partial D_1} G(\boldsymbol{\kappa},\omega;\varepsilon(\mathbf{x}-\mathbf{y}))\varphi(\mathbf{y})\, ds_{\mathbf{y}}, \quad \mathbf{x} \in \partial D_1. \tag{2.7}$$

We seek for eigenpairs (ω, φ) such that (2.6) attains nontrivial solutions.

3. Dirac point on ΓX. We consider $\boldsymbol{\kappa} = (\kappa, 0) \in \Gamma X$. In particular, we restrict our attention to the Bloch wavenumber $\boldsymbol{\kappa}$ for which $\kappa \in I_\varepsilon$, the $O(\varepsilon)$ neighborhood of $\frac{\pi}{2}$. Assume that the lattice constant $a = 1$ and D_1 is a disk with radius 1. Decompose the function space $\mathcal{H}^s(\partial D_1) = \mathcal{H}_o^s(\partial D_1) \oplus \mathcal{H}_e^s(\partial D_1)$, where $\mathcal{H}_o^s(\partial D_1)$ and $\mathcal{H}_e^s(\partial D_1)$ are subspaces of $\mathcal{H}^s(\partial D_1)$ with functions that are odd and even with respect to the x_1 axis respectively. Using the symmetry of the Green's function, we have the following lemma.

LEMMA 3.1. *$\mathcal{S}_\varepsilon^{\boldsymbol{\kappa},\omega}$ is a bounded linear operator from $\mathcal{H}_o^{-1/2}(\partial D_1)$ to $\mathcal{H}_o^{1/2}(\partial D_1)$ and $\mathcal{H}_e^{-1/2}(\partial D_1)$ to $\mathcal{H}_e^{1/2}(\partial D_1)$ respectively.*

3.1. Eigenvalues as the characteristic values of an infinite linear system. Let $\mathbb{N}_o$ be the set of the positive integers and $\mathbb{N}_e := \mathbb{N}_o \cup \{0\}$. Define

$$\mathbb{H}_i^s := \Big\{ \{a_n\}_{n\in\mathbb{N}_i} \colon \sum_{n\in\mathbb{N}_i} (1+n^2)^s |a_n|^2 < \infty \Big\} \quad (i = o, e).$$

We parameterize the boundary of D_1 by $\mathbf{r}(t) = (\cos t, \sin t)$ and introduce the functions $\phi_n^{(o)} = \frac{1}{\sqrt{\pi}}\sin(n\pi t)$ for $n \in \mathbb{N}_o$, $\phi_0^{(e)} = \frac{1}{\sqrt{2\pi}}$, and $\phi_n^{(e)} = \frac{1}{\sqrt{\pi}}\cos(n\pi t)$ for $\mathbb{N}_e\backslash\{0\}$. Define the two subspaces of $\mathcal{H}^s[(0,2\pi)]$ as follows:

$$\mathcal{H}_i^s[(0,2\pi)] := \Big\{ \sum_{n\in\mathbb{N}_i} a_n\phi_n^{(i)} \colon \{a_n\}_{n\in\mathbb{N}_i} \in \mathbb{H}_i^{-1/2} \Big\} \quad (i = o, e).$$

In view of Lemma 3.1, the linear operator $\mathcal{S}_\varepsilon^{\boldsymbol{\kappa},\omega}$ induces a bounded operator from $\mathcal{H}_i^{-1/2}([0,2\pi])$ to $\mathcal{H}_i^{1/2}([0,2\pi])$ in the parameter space for $i = e, o$, which we still denote as $\mathcal{S}_\varepsilon^{\boldsymbol{\kappa},\omega}$ for ease of notation. If we expand $\varphi \in \mathcal{H}_i^{-1/2}([0,2\pi])$ as $\varphi = \sum_{n\in\mathbb{N}_i} c_n\phi_n^{(i)}$, then (2.6) reads $\sum_{n\in\mathbb{N}_i} c_n \left(\mathcal{S}_\varepsilon^{\boldsymbol{\kappa},\omega}\phi_n^{(i)}\right) = 0$. Define the infinite matrix $\mathcal{A}_i = [a_{mn}^{(i)}]_{m,n\in\mathbb{N}_i}$, where

$$a_{mn}^{(i)}(\boldsymbol{\kappa},\omega) = \left(\mathcal{S}_\varepsilon^{\boldsymbol{\kappa},\omega}\phi_n^{(i)}, \phi_m^{(i)}\right) := \int_0^{2\pi} [\mathcal{S}_\varepsilon^{\boldsymbol{\kappa},\omega}\phi_n^{(i)}](t)\,\phi_m^{(i)}(t)\,dt. \tag{3.1}$$

We see that, when $\mathcal{S}_\varepsilon^{\boldsymbol{\kappa},\omega}$ is restricted to $\mathcal{H}_i^{-1/2}([0,2\pi])$, (2.6) holds if and only if there exists nonzero $\mathbf{c} = \{c_n\}_{n\in\mathbb{N}_i} \in \mathbb{H}_i^{-1/2}$ such that the following infinite linear system holds:

$$\mathcal{A}_i(\boldsymbol{\kappa},\omega)\,\mathbf{c} = \mathbf{0} \quad (i = o, e). \tag{3.2}$$

Such ω are called the characteristic values of the system. To study the eigenvalues ω of the Dirichlet problem (1.3a)-(1.3b), we investigate the characteristic values of (3.2). To this end, we follow the method in [22] by performing the asymptotic analysis of the integral operator to reduce (3.2) to a finite-dimensional nonlinear characteristic system and deriving the asymptotic expansions of the characteristic values with respect to the size of the obstacles ε. It is shown that each eigenvalue ω^* is near a singular frequency associated with the Green's function (2.3). These singular frequencies also correspond to the eigenvalues of the homogeneous medium over the square lattice.

3.2. Decomposition of the Green's function and the single-layer operator $\mathcal{S}_\varepsilon^{\boldsymbol{\kappa},\omega}$. Recall that $\boldsymbol{\kappa} = (\kappa, 0)$, where κ lies in the $O(\varepsilon)$ neighborhood of $\frac{\pi}{2}$. We are interested in the spectral properties near the desired location $(\boldsymbol{\kappa}^*, \omega^*)$ where $\boldsymbol{\kappa}^* = (\frac{\pi}{2}, 0)$ and $\omega^* = \frac{5\pi}{2}$. Define $\Lambda_0^* = \{\mathbf{q}_1, \mathbf{q}_2, \mathbf{q}_3\}$, where $\mathbf{q}_1 = 2\pi(-1,-1)^T$, $\mathbf{q}_2 = 2\pi(-1,1)^T$, and $\mathbf{q}_3 = 2\pi(1,0)^T$. We consider eigenvalues in the vicinity of the singular frequency $\omega = |\boldsymbol{\kappa} + \mathbf{q}|$ for $\mathbf{q} \in \Lambda_0^*$. To this end, we define the region

$$\Omega_\varepsilon(\boldsymbol{\kappa}) := \bigcup_{\mathbf{q}\in\Lambda_0^*} \{\omega \in \mathbb{R}^+ \colon C_1\varepsilon^2 \le \omega^2 - |\boldsymbol{\kappa} + \mathbf{q}|^2 \le C_2\varepsilon^2\}$$

for some positive constants C_1 and C_2.

We decompose the Green's function into the three parts as follows:

$$H_0(\omega;\mathbf{x}) := -\frac{\imath}{4}H_0^{(1)}(\omega|\mathbf{x}|), \quad \mathbf{x} \neq 0, \tag{3.3}$$

$$G_{\Lambda_0^*}(\boldsymbol{\kappa},\omega;\mathbf{x}) := \sum_{\mathbf{q}\in\Lambda_0^*} \frac{e^{\imath(\boldsymbol{\kappa}+\mathbf{q})\cdot\mathbf{x}}}{\omega^2 - |\boldsymbol{\kappa}+\mathbf{q}|^2}, \tag{3.4}$$

$$\tilde{G}(\boldsymbol{\kappa},\omega;\mathbf{x}) := G(\boldsymbol{\kappa},\omega;\mathbf{x}) - H_0(\omega;\mathbf{x}) - G_{\Lambda_0^*}(\boldsymbol{\kappa},\omega;\mathbf{x}), \quad \mathbf{x} \neq 0, \tag{3.5}$$

$$\tilde{G}(\boldsymbol{\kappa},\omega;0) := \lim_{\mathbf{x}\to 0} \tilde{G}(\boldsymbol{\kappa},\omega;\mathbf{x}).$$

In the above decomposition, $H_0(\omega;\mathbf{x})$ is singular when $|\mathbf{x}|=0$, and we introduce $G_{\Lambda_0^*}$ to extract the singular behavior of the Green's function when ω is close to the singular frequency $\omega^*=\frac{5\pi}{2}$. As such $\tilde{G}(\boldsymbol{\kappa},\omega;\mathbf{x})$ is a smooth function of $\mathbf{x}$ for any real-valued ω.

LEMMA 3.2. *([13, p.31-32, Section 2.1.1]), If $0<|\mathbf{x}|\ll 1$, then*

$$H_0(\omega;\mathbf{x})=\frac{1}{2\pi}\left[\ln|\mathbf{x}|+\ln\omega+\gamma_0+\ln(\omega|\mathbf{x}|)\sum_{p\geq 1}b_{p,1}(\omega|\mathbf{x}|)^{2p}+\sum_{p\geq 1}b_{p,2}(\omega|\mathbf{x}|)^{2p}\right],$$

where $b_{p,1}=\dfrac{(-1)^p}{2^{2p}(p!)^2}$, $b_{p,2}=\left(\gamma_0-\displaystyle\sum_{s=1}^{p}\frac{1}{s}\right)b_{p,1}$, $\gamma_0=E_0-\ln 2-\dfrac{\imath\pi}{2}$, *and*

$E_0=\displaystyle\lim_{N\to\infty}\left(\sum_{p=1}^{N}\frac{1}{p}-\ln N\right)\approx 0.57721$ *is the Euler-Mascheroni constant.*

Let U_ε be a disk centered at the origin and radius ε. From the Taylor expansion of the finite-sum $G_{\Lambda_0^*}(\mathbf{x})$, we have the following lemma.

LEMMA 3.3. *For each $\omega\in\Omega_\varepsilon(\boldsymbol{\kappa})$, $G_{\Lambda_0^*}(\boldsymbol{\kappa},\omega;\mathbf{x})$ is analytic for $\mathbf{x}\in U_{2\varepsilon}$ with $\varepsilon\ll 1$ and it possesses the Taylor expansion*

$$G_{\Lambda_0^*}(\boldsymbol{\kappa},\omega;\mathbf{x})=\frac{1}{\omega^2-\kappa_-^2-b^2}\left(2+2\imath\kappa_- x_1-(\kappa_-^2x_1^2+b^2x_2^2)\right) \tag{3.6}$$

$$+\frac{1}{\omega^2-\kappa_+^2}\left(1+\imath\kappa_+x_1-\frac{1}{2}\kappa_+^2x_1^2\right)+G^{\infty}_{\Lambda_0^*}(\boldsymbol{\kappa},\omega;\mathbf{x}), \tag{3.7}$$

where $\kappa_\pm:=\kappa\pm 2\pi$, $b:=2\pi$, and

$$G^{\infty}_{\Lambda_0^*}(\boldsymbol{\kappa},\omega;\mathbf{x})=\frac{1}{\omega^2-\kappa_-^2-b^2}\sum_{|\alpha|\geq 3}c_{\alpha_1,-}(\omega)x_1^{\alpha_1}x_2^{\alpha_2}+\frac{1}{\omega^2-\kappa_+^2}\sum_{\alpha_1\geq 3}c_{\alpha_1,+}(\omega)x_1^{\alpha_1},$$

$\alpha=(\alpha_1,\alpha_2)$, $|c_{\alpha,\pm}|<C^{|\alpha|}$ for a certain constant C independent of ω, ε and α.

LEMMA 3.4. *For each $\omega\in\Omega_\varepsilon(\boldsymbol{\kappa})$, $\tilde{G}(\boldsymbol{\kappa},\omega;\mathbf{x})$ is smooth for $\mathbf{x}\in U_{2\varepsilon}$ with $\varepsilon\ll 1$. In addition,*

$$\sup_{\omega\in\Omega_\varepsilon(\boldsymbol{\kappa})}\left|\partial_{x_1}^{\alpha_1}\partial_{x_2}^{\alpha_2}\tilde{G}(\boldsymbol{\kappa},\omega;0)\right|\leq C,\quad 0\leq\alpha_1+\alpha_2\leq 2, \tag{3.8}$$

wherein the constant C is independent of ω, ε.

DEFINITION 3.5 (Decomposition of the single-layer operator $\mathcal{S}_\varepsilon^{\boldsymbol{\kappa},\omega}$). *Let $\mathcal{S}_{H_0,\varepsilon}$, $\mathcal{S}_{\Lambda_0^*,\varepsilon}$ and $\tilde{\mathcal{S}}_\varepsilon$ be the integral operators with the kernel H_0, $G_{\Lambda_0^*}$ and $\tilde{G}$ given in (3.3)-(3.5):*

$$[\mathcal{S}_{H_0,\varepsilon}\varphi](\mathbf{x}):=\int_{\mathbf{y}\in\partial D_1}H_0(\omega;\varepsilon(\mathbf{x}-\mathbf{y}))\varphi(\mathbf{y})\,ds_{\mathbf{y}},\quad \mathbf{x}\in\partial D_1,$$

$$[\mathcal{S}_{\Lambda_0^*,\varepsilon}\varphi](\mathbf{x}):=\int_{\mathbf{y}\in\partial D_1}G_{\Lambda_0^*}(\boldsymbol{\kappa},\omega;\varepsilon(\mathbf{x}-\mathbf{y}))\varphi(\mathbf{y})\,ds_{\mathbf{y}},\quad \mathbf{x}\in\partial D_1,$$

$$[\tilde{\mathcal{S}}_\varepsilon\varphi](\mathbf{x}):=\int_{\mathbf{y}\in\partial D_1}\tilde{G}(\boldsymbol{\kappa},\omega;\varepsilon(\mathbf{x}-\mathbf{y}))\varphi(\mathbf{y})\,ds_{\mathbf{y}},\quad \mathbf{x}\in\partial D_1.$$

Then, it follows that $\mathcal{S}_\varepsilon^{\boldsymbol{\kappa},\omega}=\mathcal{S}_{H_0,\varepsilon}+\mathcal{S}_{\Lambda_0^*,\varepsilon}+\tilde{\mathcal{S}}_\varepsilon$.

3.3. Decomposition of the matrix $\mathcal{A}_i$. Recall that $a_{mn}^{(i)} = \left(\mathcal{S}_\varepsilon^{\boldsymbol{\kappa},\omega}\phi_n^{(i)}, \phi_m^{(i)}\right)$, using the decomposition of the integral operator $\mathcal{S}_\varepsilon^{\boldsymbol{\kappa},\omega}$, we express $a_{mn}^{(i)}$ as the sum of the following three terms:

$$(\mathcal{S}_{H_0,\varepsilon})_{mn}^{(i)} := \left(\mathcal{S}_{H_0,\varepsilon}\phi_n^{(i)}, \phi_m^{(i)}\right),\ (\mathcal{S}_{\Lambda_0^*,\varepsilon})_{mn}^{(i)} := \left(\mathcal{S}_{\Lambda_0^*,\varepsilon}\phi_n^{(i)}, \phi_m^{(i)}\right),\ (\tilde{\mathcal{S}}_\varepsilon)_{mn}^{(i)} := \left(\tilde{\mathcal{S}}_\varepsilon\phi_n^{(i)}, \phi_m^{(i)}\right).$$

In what follows, we obtain the asymptotic expansion of $(\mathcal{S}_{H_0,\varepsilon})_{mn}^{(i)}$, $(\mathcal{S}_{\Lambda_0^*,\varepsilon})_{mn}^{(i)}$, and $(\tilde{\mathcal{S}}_\varepsilon)_{mn}^{(i)}$ to obtain a decomposition of the matrix $\mathcal{A}_i$.

3.3.1. The decomposition for $\mathcal{A}_o$. Recall that $\phi_n^{(o)} = \frac{1}{\sqrt{\pi}}\sin(n\pi t)$ for $n \in \mathbb{N}_o$. In light of the expansions in Lemmas 3.2, 3.3 and 3.4, we obtain the following expansions for $(\mathcal{S}_{H_0,\varepsilon})_{mn}^{(o)}$, $(\mathcal{S}_{\Lambda_0^*,\varepsilon})_{mn}^{(o)}$, and $(\tilde{\mathcal{S}}_\varepsilon)_{mn}^{(o)}$.

LEMMA 3.6. *For $\varepsilon \ll 1$, there holds*

$$(\mathcal{S}_{H_0,\varepsilon})_{mn}^{(o)} = \begin{cases} -\dfrac{1}{2n}\left(1 + O(\varepsilon^2\ln\varepsilon)\right) & m = n \in \mathbb{N}_o, \\ 0 & \text{otherwise.} \end{cases} \tag{3.9}$$

Proof. Define

$$\mathcal{S}_0\varphi(\mathbf{x}) := \frac{1}{2\pi}\int_{\mathbf{y}\in\partial D_1} \ln|\mathbf{x}-\mathbf{y}|\,\varphi(\mathbf{y})\,ds_{\mathbf{y}}, \quad \mathbf{x} \in \partial D_1. \tag{3.10}$$

On the unit circle, there holds $|\mathbf{x}-\mathbf{y}|^2 = |\mathbf{r}(t)-\mathbf{r}(\tau)|^2 = 2-2\cos(t-\tau) = 4\sin^2\left(\frac{t-\tau}{2}\right)$. As such, in the parameter space, it follows from Lemma 8.23 in [16] that

$$[\mathcal{S}_0\psi_n](t) = \frac{1}{4\pi}\int_0^{2\pi} \ln\left(4\sin^2\left(\frac{t-\tau}{2}\right)\right)\psi_n(\tau)\,d\tau = \eta_n\psi_n(t), \tag{3.11}$$

where

$$\eta_n = \begin{cases} 0, & n = 0; \\ -\frac{1}{2|n|}, & n \neq 0; \end{cases} \quad \text{and} \quad \psi_n(t) = \frac{1}{\sqrt{2\pi}}e^{\imath nt}.$$

Therefore, using the relation $\phi_n^{(o)}(t) = \frac{1}{\sqrt{2}\imath}(\psi_n(t)-\psi_{-n}(t))$, the expansion (3.9) follows from (3.11) and Lemma 3.2. ∎

A direction computation under the polar coordinate by using Lemma 3.3 leads to the following expansions.

LEMMA 3.7. *For $\varepsilon \ll 1$ and $\omega \in \Omega_\varepsilon(\boldsymbol{\kappa})$, there holds*

$$(\mathcal{S}_{\Lambda_0^*,\varepsilon})_{mn}^{(o)} = \begin{cases} \dfrac{1}{\omega^2-\kappa_-^2-b^2}\left(2\pi b^2\varepsilon^2 + O(\varepsilon^3)\right) & m = n = 1, \\ \left(\dfrac{1}{\omega^2-\kappa_-^2-b^2} + \dfrac{1}{\omega^2-\kappa_+^2}\right) O\left(\varepsilon^{\max(3,|m|,|n|)}\right) & \text{otherwise.} \end{cases} \tag{3.12}$$

LEMMA 3.8. *For $\varepsilon \ll 1$ and $\omega \in \Omega_\varepsilon(\boldsymbol{\kappa})$, $(\tilde{\mathcal{S}}_\varepsilon)_{mn}^{(o)} = \varepsilon\tilde{a}_{mn}$ where the operator $\tilde{\mathcal{A}} := [\tilde{a}_{mn}]$ is bounded from $\mathbb{H}_o^{-1/2}$ to $\mathbb{H}_o^{1/2}$, and the operator norm $\|\tilde{\mathcal{A}}\| \leq C$ with C independent of ε and ω.*

Note that for $\omega \in \Omega_\varepsilon(\boldsymbol{\kappa})$, there holds $\dfrac{1}{|\omega^2-\kappa_-^2-b^2|}$, $\dfrac{1}{|\omega^2-\kappa_+^2|} \sim O\left(\frac{1}{\varepsilon^2}\right)$. Therefore, by virtue of Lemmas 3.6–3.8, we obtain the following decomposition for the matrix $\mathcal{A}_o$:

PROPOSITION 3.9 (Decomposition of $\mathcal{A}_o$). *There exists a constant $\mathsf{c}>0$ such that for $\varepsilon \in (0,\mathsf{c})$ and $\omega \in \Omega_\varepsilon(\boldsymbol{\kappa})$, the matrix $\mathcal{A}$ can be decomposed as $\mathcal{A}_o = \mathcal{D}_o + \varepsilon\,\mathcal{E}_o + o(\varepsilon)$, where $\mathcal{D}_o := \mathrm{diag}(d_n)_{n\in\mathbb{Z}}$ with*

$$d_n = \begin{cases} \dfrac{2\pi b^2\varepsilon^2}{\omega^2-\kappa_-^2-b^2} - \dfrac{1}{2} & n=1, \\ -\dfrac{1}{2n}, & n>1, \end{cases}$$

and $\mathcal{E}_o = [e_{mn}]$. In addition, $\mathcal{E}_o$ is bounded from $\mathbb{H}_o^{-1/2}$ to $\mathbb{H}_o^{1/2}$ with the norm $\|\mathcal{E}_o\| \le C$ for a constant C independent of ε and ω.

3.3.2. The decomposition for $\mathcal{A}_e$. Following the procedure in Section 3.3.1, we can obtain the similar decomposition for $\mathcal{A}_e$ by noting that $\phi_0^{(e)} = \frac{1}{\sqrt{2\pi}}$ and $\phi_n^{(e)} = \frac{1}{\sqrt{\pi}}\cos(n\pi t)$ for $n \ge 1$.

LEMMA 3.10. *For $\varepsilon \ll 1$, there holds*

$$(\mathcal{S}_{H_0,\varepsilon})_{mn}^{(e)} = \begin{cases} \dfrac{1}{2\pi}(\ln\varepsilon + \ln\omega + \gamma_0) + O(\varepsilon^2\ln\varepsilon) & m=n=0, \\ -\dfrac{1}{2n}\left(1+O(\varepsilon^2\ln\varepsilon)\right) & m=n\ge 1, \\ 0 & m\ne n. \end{cases} \tag{3.13}$$

Let $\mathcal{Q} = [q_{mn}]_{m,n=0}^{\infty}$ be an infinite matrix, for which the nonzero elements are

$$\begin{aligned} q_{00} &= 2\pi\left(\frac{2}{\omega^2-\kappa_-^2-b^2} + \frac{1}{\omega^2-\kappa_+^2}\right) - 2\pi\varepsilon^2\left(\frac{\kappa_-^2+b^2}{\omega^2-\kappa_-^2-b^2} + \frac{1}{2}\frac{\kappa_+^2}{\omega^2-\kappa_+^2}\right), \\ q_{01} &= \sqrt{2}\pi\varepsilon\left(\frac{2\imath\kappa_-}{\omega^2-\kappa_-^2-b^2} + \frac{\imath\kappa_+}{\omega^2-\kappa_+^2}\right), \quad q_{10} = -q_{01}, \\ q_{02} &= \frac{\pi\varepsilon^2}{\sqrt{2}}\left(\frac{\kappa_-^2+b^2}{\omega^2-\kappa_-^2-b^2} + \frac{1}{2}\frac{\kappa_+^2}{\omega^2-\kappa_+^2}\right), \quad q_{20} = q_{02}, \\ q_{11} &= 2\pi\varepsilon^2\left(\frac{\kappa_-^2}{\omega^2-\kappa_-^2-b^2} + \frac{1}{2}\frac{\kappa_+^2}{\omega^2-\kappa_+^2}\right), \end{aligned}$$

LEMMA 3.11. *For $\varepsilon \ll 1$ and $\omega \in \Omega_\varepsilon(\boldsymbol{\kappa})$, there holds*

$$(\mathcal{S}_{\Lambda_0^*,\varepsilon})_{mn}^{(e)} = q_{mn} + \left(\frac{1}{\omega^2-\kappa_-^2-b^2} + \frac{1}{\omega^2-\kappa_+^2}\right) O\left(\varepsilon^{\max(3,|m|,|n|)}\right). \tag{3.14}$$

LEMMA 3.12. *For $\varepsilon \ll 1$ and $\omega \in \Omega_\varepsilon(\boldsymbol{\kappa})$, $(\tilde{\mathcal{S}}_\varepsilon)_{mn}$ can be expressed as*

$$(\tilde{\mathcal{S}}_\varepsilon)_{mn}^{(e)} = \begin{cases} \tilde{G}(\boldsymbol{\kappa},\omega;\mathbf{0}) + \varepsilon\cdot\tilde{a}_{00} & m=n=0, \\ \varepsilon\cdot\tilde{a}_{mn} & \textit{otherwise}, \end{cases} \tag{3.15}$$

where the operator $\tilde{\mathcal{A}} := [\tilde{a}_{mn}]$ *is bounded from* $\mathbb{H}_e^{-1/2}$ *to* $\mathbb{H}_e^{1/2}$*, and the operator norm* $\|\tilde{\mathcal{A}}\| \le C$ *with* C *independent of* ε *and* ω*.*

Therefore, by virtue of Lemmas 3.10 - 3.12, we obtain the following decomposition for the matrix $\mathcal{A}_e$:

PROPOSITION 3.13 (Decomposition of $\mathcal{A}_e$). *There exists a constant* $\mathsf{c} > 0$ *such that for* $\varepsilon \in (0, \mathsf{c})$ *and* $\omega \in \Omega_\varepsilon(\boldsymbol{\kappa})$*, the matrix* $\mathcal{A}_e$ *can be decomposed as* $\mathcal{A}_e = \mathcal{Q} + \mathcal{D}_e + \varepsilon\,\mathcal{E}_e + o(\varepsilon)$*, where* $\mathcal{D}_e := \operatorname{diag}(d_n)_{n\in\mathbb{Z}}$ *with*

$$d_n = \begin{cases} \dfrac{1}{2\pi}(\ln\varepsilon + \ln\omega + \gamma_0)) + \tilde{G}(\boldsymbol{\kappa}, \omega; \mathbf{0}) & n = 0, \\ -\dfrac{1}{2n}, & n > 1, \end{cases}$$

and $\mathcal{E}_e = [e_{mn}]$*. In addition,* $\mathcal{E}_e$ *is bounded from* $\mathbb{H}_e^{-1/2}$ *to* $\mathbb{H}_e^{1/2}$ *with the norm* $\|\mathcal{E}_e\| \le C$ *for a constant* C *independent of* ε *and* ω*.*

3.4. Characteristic equations. We reduce the systems (3.2) to the nonlinear characteristic equations for ω by using the decomposition of the matrix $\mathcal{A}_i$ in Proposition 3.9 and 3.13.

For $i = o$, we denote $\mathbb{N}^* = \mathbb{N}_o\backslash\{1\}$ and define the vectors $\hat{\mathbf{a}}_o := \{a_{m1}^{(o)}\}_{m\in\mathbb{N}^*}$, $\hat{\mathbf{c}} := \{c_m\}_{m\in\mathbb{N}^*}$, and the matrix $\hat{\mathcal{A}}_o := [a_{mn}^{(o)}]_{m\in\mathbb{N}^*, n\in\mathbb{N}^*}$. Then the system (3.2) can be split into the following two equations:

$$a_{11}^{(o)}\, c_1 + \hat{\mathbf{a}}_o^*\hat{\mathbf{c}} = 0, \quad c_1\hat{\mathbf{a}}_o + \hat{\mathcal{A}}_o\hat{\mathbf{c}} = \mathbf{0}. \tag{3.16}$$

LEMMA 3.14. *For* $\omega \in \Omega_\varepsilon(\boldsymbol{\kappa})$ *and sufficiently small* ε*, the operator* $\hat{\mathcal{A}}_o \colon \mathcal{H}_o^{-1/2} \to \mathcal{H}_o^{1/2}$ *is invertible.*

Proof. For each $\omega \in \Omega_\varepsilon(\boldsymbol{\kappa})$, let $\hat{\mathcal{A}}_o$ be decomposed as $\hat{\mathcal{A}}_o = \hat{\mathcal{D}}_o + \varepsilon\hat{\mathcal{E}}_o + o(\varepsilon)$ using the decomposition of $\mathcal{A}_o$ in Proposition 3.9. Using the explicit expression of $\{d_n\}_{n=2}^{\infty}$ in Proposition 3.9, it can be shown that $\hat{\mathcal{D}}_o$ is invertible from $\mathbb{H}_o^{-1/2}$ to $\mathbb{H}_o^{1/2}$ with a bounded operator norm $\|\hat{\mathcal{D}}_o^{-1}\|$. Expressing $\hat{\mathcal{A}}_o$ as $\hat{\mathcal{A}}_o = \hat{\mathcal{D}}_o(I + \varepsilon\hat{\mathcal{D}}_o^{-1}\hat{\mathcal{E}}_o + o(\varepsilon))$, then it is clear that $\hat{\mathcal{A}}_o$ is invertible for sufficiently small ε. ∎

Using Lemma 3.14, we express $\hat{\mathbf{c}}$ as $\hat{\mathbf{c}} = -c_1(\hat{\mathcal{A}}_o^{-1}\hat{\mathbf{a}}_o)$ and substitute into the first equation in (3.16) to obtain

$$\left(a_{11}^{(o)} - \hat{\mathbf{a}}_o^*\hat{\mathcal{A}}_o^{-1}\hat{\mathbf{a}}_o\right) c_1 = 0. \tag{3.17}$$

Similarly, for $i = e$, by expressing the vector $\mathbf{c}$ as $\mathbf{c} = [\mathbf{c}_1, \mathbf{c}_2]$ and the matrix $\mathcal{A}_e$ as

$$\mathcal{A}_e = \begin{pmatrix} \mathcal{A}_{e,11} & \mathcal{A}_{e,21}^* \\ \mathcal{A}_{e,21} & \mathcal{A}_{e,22} \end{pmatrix},$$

where $\mathbf{c}_1 = [c_0, c_1, c_2]^T$ and $\mathcal{A}_{e,11}$ is 3×3 matrix, the system (3.2) can be reduced to

$$\left(\mathcal{A}_{e,11} - \mathcal{A}_{e,21}^*\hat{\mathcal{A}}_{e,22}^{-1}\mathcal{A}_{e,21}\right)\mathbf{c}_1 = 0. \tag{3.18}$$

To obtain the characteristic values of (3.2) for each $\boldsymbol{\kappa}$, we solve for ω such that (3.17) and (3.18) attain nontrivial solutions, or equivalently, we find ω that is a root

of one of the following characteristic equations:

$$a_{11}^{(o)}(\boldsymbol{\kappa},\omega) - \hat{\mathbf{a}}_o^*(\boldsymbol{\kappa},\omega)\hat{\mathcal{A}}_o^{-1}(\boldsymbol{\kappa},\omega)\hat{\mathbf{a}}_o(\boldsymbol{\kappa},\omega) = 0, \tag{3.19a}$$

$$\det\left(\mathcal{A}_{e,11}(\boldsymbol{\kappa},\omega) - \mathcal{A}_{e,21}^*(\boldsymbol{\kappa},\omega)\hat{\mathcal{A}}_{e,22}^{-1}(\boldsymbol{\kappa},\omega)\mathcal{A}_{e,21}(\boldsymbol{\kappa},\omega)\right) = 0. \tag{3.19b}$$

3.5. Degeneracy of the eigenvalue. We solve the characteristic equations (3.19a) and (3.19b) to obtain the eigenvalues. From Proposition 3.9, we have

$$a_{11}^{(o)}(\boldsymbol{\kappa},\omega) = \frac{2\pi b^2\varepsilon^2}{\omega^2-\kappa_-^2-b^2} - \frac{1}{2} + O(\varepsilon); \quad a_{m1}^{(o)} = \varepsilon e_{m1}^{(o)} + o(\varepsilon), \quad m > 1.$$

In light of Proposition 3.9, (3.19a) reads

$$\frac{2\pi b^2\varepsilon^2}{\omega^2-\kappa_-^2-b^2} - \frac{1}{2} + O(\varepsilon) = 0.$$

Hence the corresponding root ω_o satisfies

$$\omega_o^2 = \kappa_-^2 + b^2 + 4\pi b^2\varepsilon^2\left(1+O(\varepsilon)\right). \tag{3.20}$$

Similarly, let $\beta = \frac{1}{2\pi}(\ln\omega+\gamma_0)) + \tilde{G}(\boldsymbol{\kappa},\omega;\mathbf{0})$, it follows from Proposition 3.13 that

$$\begin{aligned} a_{00}^{(e)} &= q_{00} + \frac{1}{2\pi}\ln\varepsilon + \beta + O(\varepsilon);\\ a_{mn}^{(e)} &= q_{mn} - \frac{1}{2n}\delta_{mn} + \varepsilon e_{mn}^{(e)} + o(\varepsilon) \quad \text{otherwise.}\end{aligned}$$

An explicit evaluation of the characteristic equation (3.19b) yields

$$\begin{aligned}&\left(\frac{2}{\omega^2-\kappa_-^2-b^2}+\frac{1}{\omega^2-\kappa_+^2}\right)\cdot\left(1+O\left(\varepsilon^2\ln\varepsilon\right)\right) + 4\pi^2\varepsilon^2\left(\frac{2\kappa_-}{\omega^2-\kappa_-^2-b^2}+\frac{\kappa_+}{\omega^2-\kappa_+^2}\right)^2\\ &-8\pi^2\varepsilon^2\left(\frac{2}{\omega^2-\kappa_-^2-b^2}+\frac{1}{\omega^2-\kappa_+^2}\right)\left(\frac{\kappa_-^2}{\omega^2-\kappa_-^2-b^2}+\frac{1}{2}\frac{\kappa_+^2}{\omega^2-\kappa_+^2}\right)+\frac{\ln\varepsilon}{2\pi}+\beta+O(\varepsilon)=0,\end{aligned}$$

which can be simplified as

$$\left(\frac{2}{\omega^2-\kappa_-^2-b^2}+\frac{1}{\omega^2-\kappa_+^2}\right)\cdot\left(1+O\left(\varepsilon^2\ln\varepsilon\right)\right)-\frac{8\pi^2\varepsilon^2(\kappa_+-\kappa_-)^2}{(\omega^2-\kappa_-^2-b^2)\cdot(\omega^2-\kappa_+^2)}+\frac{\ln\varepsilon}{2\pi}+\beta+O(\varepsilon)=0.$$

Equivalently, the equation can be written as

$$\left(2(\omega^2-\kappa_+^2)+(\omega^2-\kappa_-^2-b^2)\right)\cdot\left(1+O\left(\varepsilon^2\ln\varepsilon\right)\right)-128\pi^4\varepsilon^2+\left(\frac{\ln\varepsilon}{2\pi}+\beta+O(\varepsilon)\right)\cdot(\omega^2-\kappa_-^2-b^2)\cdot(\omega^2-\kappa_+^2)=0.$$

In particular, the above equation holds when $\omega^2-\kappa_-^2-b^2=0$ or $\omega^2-\kappa_+^2=0$. The corresponding root $\omega_e(\kappa)$ satisfies

$$\omega_e^2(\kappa) = \kappa_-^2 + b^2 = \kappa_+^2 + 64\pi^4\varepsilon^2\left(1+O(\varepsilon^2\ln\varepsilon)\right), \tag{3.21}$$

$$\omega_e^2(\kappa) = \kappa_+^2 = \kappa_-^2 + b^2 + 128\pi^4\varepsilon^2\left(1+O(\varepsilon^2\ln\varepsilon)\right), \tag{3.22}$$

with $\kappa = \underline{\kappa} = \frac{\pi}{2} - 8\pi^3\varepsilon^2 + O(\varepsilon^3\ln\varepsilon)$ and $\kappa = \bar{\kappa} = \frac{\pi}{2} + 16\pi^3\varepsilon^2 + O(\varepsilon^3\ln\varepsilon)$, respectively.

By virtue of (3.20) -(3.22), we see that

$$\omega_o(\underline{\kappa}) - \omega_e(\underline{\kappa}) > 0 \quad \text{and} \quad \omega_o(\bar{\kappa}) - \omega_e(\bar{\kappa}) < 0 \tag{3.23}$$

for sufficiently small ε. The continuity of the band frequency leads to the degeneracy of the eigenvalues with $\omega_o(\kappa^*) = \omega_e(\kappa^*)$ for some $\kappa^* \in (\underline{\kappa}, \bar{\kappa})$. The corresponding eigenfunctions can be solved by (3.17) and (3.18).

THEOREM 3.15. *There exists $\kappa^* \in (\underline{\kappa}, \bar{\kappa})$ such that $\omega_o(\kappa^*) = \omega_e(\kappa^*) = \omega^*$ is a characteristic value of (2.6). Furthermore, ω^* attains the asymptotic expansion (3.20), with the corresponding two-dimensional eigenspace $\mathcal{H}_*^{-1/2}(\partial D_1)$ spanned by $\phi_o(\mathbf{x}) = x_2 + O(\varepsilon x^\alpha) \in \mathcal{H}_o^{-1/2}(\partial D_1)$ and $\phi_e(\mathbf{x}) = \alpha_0 \varepsilon + x_1 + O(\varepsilon x^\alpha) \in \mathcal{H}_e^{-1/2}(\partial D_1)$, wherein α_0 is a nonzero constant independent of ε and $|\alpha| = 2$.*

REMARK 3.16. *We observe from (3.23) that $\omega_o(\kappa) - \omega_e(\kappa)$ swaps signs at $\underline{\kappa}$ and $\bar{\kappa}$. Indeed, it can be shown that the sign of $\omega_o(\kappa) - \omega_e(\kappa)$ swaps when $\kappa < \kappa^*$ and $\kappa > \kappa^*$ near κ^*. Namely, the two branches of eigenvalues with different parity of eigenfunctions cross each other at κ^*.*

REMARK 3.17. *From the analysis above, it is observed that the Bloch wavenumber κ^* at the degeneracy point depends on the perturbation parameter ε. Furthermore, when ε is no longer small, the numerical computation implies that the degeneracy point (κ^*, ω^*) may disappear. This is very different from the Dirac point for the honeycomb lattice, where the Dirac point persists at the high symmetry point of the Brillouin zone, even for large perturbation parameter ε [7].*

3.6. The conical singularity for the dispersion surface near $(\boldsymbol{\kappa}^*, \omega^*)$. We consider the eigenpair $(\boldsymbol{\kappa}, \omega)$ near $(\boldsymbol{\kappa}^*, \omega^*)$ for the eigenvalue problem (2.6). Let $\varphi^* \in \mathcal{H}_*^{-1/2}(\partial D_1) := \text{span}\{\phi_o, \phi_e\}$ be a solution to the system $\mathcal{S}_\varepsilon^{\boldsymbol{\kappa}^*, \omega^*}\varphi = 0$. Define $\delta\boldsymbol{\kappa} = \boldsymbol{\kappa} - \boldsymbol{\kappa}^*$, $\delta\omega = \omega - \omega^*$, $\delta\varphi = \varphi - \varphi^*$, and $\delta\mathcal{S}_\varepsilon := \mathcal{S}_\varepsilon^{\boldsymbol{\kappa}, \omega} - \mathcal{S}_\varepsilon^{\boldsymbol{\kappa}^*, \omega^*}$. Then $\delta\varphi$ satisfies

$$\mathcal{S}_\varepsilon^{\boldsymbol{\kappa}^*, \omega^*}\delta\varphi = -\delta\mathcal{S}_\varepsilon\varphi^* - \delta\mathcal{S}_\varepsilon\delta\varphi. \tag{3.24}$$

The Fredholm alternative implies that (3.24) attains a solution if and only if

$$\left(\delta\mathcal{S}_\varepsilon\varphi^* + \delta\mathcal{S}_\varepsilon\delta\varphi, \phi_j\right) = 0, \quad j = o, e. \tag{3.25}$$

Under the above condition, there exists a unique $\delta\varphi \perp \mathcal{H}_*^{-1/2}(\partial D_1)$ that solves (3.24), which is given by

$$\delta\varphi = -\left(\mathcal{I} + \mathcal{S}_\perp^{-1}\delta\mathcal{S}_\varepsilon\right)^{-1}\left(\mathcal{S}_\perp^{-1}\delta\mathcal{S}_\varepsilon\right)\varphi^*. \tag{3.26}$$

Here $\mathcal{S}_\perp$ denotes the restriction of $\mathcal{S}_\varepsilon^{\boldsymbol{\kappa}^*, \omega^*}$ onto the subspace that is orthogonal to $\mathcal{H}_*^{-1/2}(\partial D_1)$. Combining (3.25) and (3.26), and expanding φ^* as $\varphi^* = \alpha_1\phi_o + \alpha_2\phi_e$ for $\alpha_1, \alpha_2 \in \mathbb{C}$, we have the following lemma for $(\boldsymbol{\kappa}, \omega)$.

LEMMA 3.18. *The pair $(\boldsymbol{\kappa}, \omega)$ in the neighborhood of $(\boldsymbol{\kappa}^*, \omega^*)$ is an eigenpair of (2.6) if and only if the following 2×2 system holds for some α_1 and α_2 satisfying $\alpha_1 \cdot \alpha_2 \neq 0$:*

$$\begin{pmatrix} \left((\mathcal{I} + \mathcal{T})\delta\mathcal{S}_\varepsilon\phi_o, \phi_o\right) & \left((\mathcal{I} + \mathcal{T})\delta\mathcal{S}_\varepsilon\phi_o, \phi_e\right) \\ \left((\mathcal{I} + \mathcal{T})\delta\mathcal{S}_\varepsilon\phi_e, \phi_o\right) & \left((\mathcal{I} + \mathcal{T})\delta\mathcal{S}_\varepsilon\phi_e, \phi_e\right) \end{pmatrix} \begin{pmatrix} \alpha_1 \\ \alpha_2 \end{pmatrix} = \begin{pmatrix} 0 \\ 0 \end{pmatrix} \tag{3.27}$$

where the operator $\mathcal{T} := -\delta\mathcal{S}_\varepsilon\left(\mathcal{I} + \mathcal{S}_\perp^{-1}\delta\mathcal{S}_\varepsilon\right)^{-1}\mathcal{S}_\perp^{-1}$.

We have the following lemma using the decomposition (3.3)-(3.5) and a standard perturbation argument.

LEMMA 3.19. *For each fixed $\varepsilon \ll 1$, near $(\boldsymbol{\kappa}^*, \omega^*)$, there holds*

$$\big(\delta\mathcal{S}_\varepsilon\phi_i, \phi_j\big) = (\delta\boldsymbol{\kappa}, \delta\omega)\cdot\Big(\big(\nabla_{\boldsymbol{\kappa},\omega}\mathcal{S}_{\Lambda_0^*,\varepsilon}\phi_i, \phi_j\big) + O(1)\Big) + O(|\delta\boldsymbol{\kappa}|^2) + O(|\delta\omega|^2) \tag{3.28}$$

for sufficiently small $\delta\boldsymbol{\kappa}$ and $\delta\omega$, where $\mathcal{S}_{\Lambda_0^*,\varepsilon}$ is introduced in Definition 3.5.

THEOREM 3.20. *Given $\varepsilon \ll 1$, there are two distinct branches of eigenvalues $\omega^\pm(\boldsymbol{\kappa})$ near $(\boldsymbol{\kappa}^*, \omega^*)$ such that $\omega^\pm(\boldsymbol{\kappa}^*) = \omega^*$ and each branch $\omega^\pm(\boldsymbol{\kappa})$ is a cone locally.*

Proof. Using Lemma 3.18 and the expansion of $\mathcal{T}$, we observe that the pair $(\boldsymbol{\kappa}, \omega)$ in the neighborhood of $(\boldsymbol{\kappa}^*, \omega^*)$ satisfies

$$\det\begin{pmatrix} \big(\delta\mathcal{S}_\varepsilon\phi_o, \phi_o\big) & \big(\delta\mathcal{S}_\varepsilon\phi_o, \phi_e\big) \\ \big(\delta\mathcal{S}_\varepsilon\phi_e, \phi_o\big) & \big(\delta\mathcal{S}_\varepsilon\phi_e, \phi_e\big) \end{pmatrix} = 0 \tag{3.29}$$

up to the first order in terms of $\delta\boldsymbol{\kappa}$ and $\delta\omega$ for each entry of the matrix. In view of Lemma 3.19, we first compute the gradient $\nabla_{\boldsymbol{\kappa},\omega}G_{\Lambda_0^*}(\boldsymbol{\kappa}^*, \omega^*; \mathbf{x})$. For each $\mathbf{q} \in \Lambda_0^*$, the partial derivative of each mode is given by

$$\begin{aligned}
\partial_{\kappa_j}\left(\frac{e^{\imath(\boldsymbol{\kappa}+\mathbf{q})\cdot\mathbf{x}}}{\omega^2 - |\boldsymbol{\kappa}+\mathbf{q}|^2}\right) &= \frac{\imath x_j e^{\imath(\boldsymbol{\kappa}+\mathbf{q})\cdot\mathbf{x}}}{\omega^2 - |\boldsymbol{\kappa}+\mathbf{q}|^2} + \frac{2(\boldsymbol{\kappa}_j + q_j)e^{\imath(\boldsymbol{\kappa}+\mathbf{q})\cdot\mathbf{x}}}{(\omega^2 - |\boldsymbol{\kappa}+\mathbf{q}|^2)^2}, \\
\partial_{\omega}\left(\frac{e^{\imath(\boldsymbol{\kappa}+\mathbf{q})\cdot\mathbf{x}}}{\omega^2 - |\boldsymbol{\kappa}+\mathbf{q}|^2}\right) &= \frac{-2\omega e^{\imath(\boldsymbol{\kappa}+\mathbf{q})\cdot\mathbf{x}}}{(\omega^2 - |\boldsymbol{\kappa}+\mathbf{q}|^2)^2}.
\end{aligned}$$

For $|\mathbf{x}| = \varepsilon$, using the Taylor expansion and the fact that $(\omega^*)^2 - |\boldsymbol{\kappa}^* + \mathbf{q}|^2 = O(\varepsilon^2)$ for $\mathbf{q} \in \Lambda_0^*$, we obtain

$$\begin{aligned}
\partial_{\kappa_1}G_{\Lambda_0^*}(\boldsymbol{\kappa}^*, \omega^*; \mathbf{x}) &= \frac{2\kappa_-^*}{((\omega^*)^2 - (\kappa_-^*)^2 - b^2)^2}\left(2 + 2\imath\kappa_-^* x_1 - \big((\kappa_-^*)^2 x_1^2 + b^2 x_2^2\big)\right) \\
&\quad + \frac{2\kappa_+^*}{((\omega^*)^2 - (\kappa_+^*)^2)^2}\left(1 + \imath\kappa_+^* x_1 - \frac{(\kappa_+^*)^2}{2}x_1^2\right) + O\left(\frac{1}{\varepsilon}\right), \\
\partial_{\kappa_2}G_{\Lambda_0^*}(\boldsymbol{\kappa}^*, \omega^*; \mathbf{x}) &= \frac{\imath 4b^2 x_2 - 4b^2\kappa^* x_1 x_2}{((\omega^*)^2 - (\kappa_-^*)^2 - b^2)^2} + O\left(\frac{1}{\varepsilon}\right), \\
\partial_{\omega}G_{\Lambda_0^*}(\boldsymbol{\kappa}^*, \omega^*; \mathbf{x}) &= \frac{-2\omega^*}{((\omega^*)^2 - (\kappa_-^*)^2 - b^2)^2}\left(2 + 2\imath\kappa_-^* x_1 - \big((\kappa_-^*)^2 x_1^2 + b^2 x_2^2\big)\right) \\
&\quad + \frac{-2\omega^*}{((\omega^*)^2 - (\kappa_+^*)^2)^2}\left(1 + \imath\kappa_+^* x_1 - \frac{(\kappa_+^*)^2}{2}x_1^2\right) + O\left(\frac{1}{\varepsilon}\right).
\end{aligned}$$

By substituting the above into (3.28) and using $\phi_o(\mathbf{x}) = x_2 + O(\varepsilon x^\alpha)$ and $\phi_e(\mathbf{x}) = \varepsilon + x_1 + O(\varepsilon x^\alpha)$, it can be computed that

$$\begin{aligned}
\big(\delta\mathcal{S}(\boldsymbol{\kappa}^*, \omega^*)\phi_o, \phi_o\big) &= b^2\lambda_-^*(\kappa_-^*\delta\kappa_1 - \omega^*\delta\omega) + s_{oo}^\infty, \\
\big(\delta\mathcal{S}(\boldsymbol{\kappa}^*, \omega^*)\phi_o, \phi_e\big) &= b^2\lambda_-^*(\kappa^* - \imath 2\alpha_0)\cdot\delta\kappa_2 + s_{oe}^\infty, \\
\big(\delta\mathcal{S}(\boldsymbol{\kappa}^*, \omega^*)\phi_e, \phi_o\big) &= b^2\lambda_-^*\varepsilon^2(\kappa^* + \imath 2\alpha_0)\cdot\delta\kappa_2 + s_{eo}^\infty, \\
\big(\delta\mathcal{S}(\boldsymbol{\kappa}^*, \omega^*)\phi_e, \phi_e\big) &= \frac{1}{2}\Big(\big(2\lambda_-^*(\kappa_-^*)^3 + \lambda_+^*(\kappa_+^*)^3\big) + 4\alpha_0^2\big(2\lambda_-^*\kappa_-^* + \lambda_+^*\kappa_+^*\big)\Big)\cdot\delta\kappa_1 \\
&\quad - \frac{\omega^*}{2}\Big(\big(2\lambda_-^*(\kappa_-^*)^2 + \lambda_+^*(\kappa_+^*)^2\big) + 4\alpha_0^2\big(2\lambda_-^* + \lambda_+^*\big)\Big)\cdot\delta\omega + s_{ee}^\infty.
\end{aligned}$$

Here, $\kappa_{\pm}^* = \kappa^* \pm 2\pi$, $\lambda_-^* = \frac{b^2\varepsilon^2}{((\omega^*)^2-(\kappa_-^*)^2-b^2)^2}$, $\lambda_+^* = \frac{b^2\varepsilon^2}{((\omega^*)^2-(\kappa_+^*)^2)^2}$, and the high-order terms are $s_{mn}^{\infty} = O\left(\frac{1}{\varepsilon}\right) + O(|\delta\boldsymbol{\kappa}|^2) + O(|\delta\omega|^2)$. Therefore, we obtain that the leading-order of the dispersion relation (3.29) is a homogeneous equation of the form

$$t_1 \cdot (\delta\omega)^2 + t_2 \cdot (\delta\kappa_1)^2 + t_3 \cdot (\delta\kappa_2)^2 + t_4 \cdot (\delta\kappa_1 \cdot \delta\omega) = 0,$$

wherein $t_1 > 0$ and $t_2, t_3 < 0$. The proof is complete. ∎

4. Dirac point on ΓM and XM.

4.1. Dirac point on ΓM. We consider $\boldsymbol{\kappa} = (\kappa, \kappa) \in \Gamma M$. With the abuse of notation, we decompose the function space $\mathcal{H}^s(\partial D_1) = \mathcal{H}_o^s(\partial D_1) \oplus \mathcal{H}_e^s(\partial D_1)$ (odd/even w.r.t. the line $x_1 = x_2$), and restrict the single layer operator $\mathcal{S}_\varepsilon^{\boldsymbol{\kappa},\omega}$ onto each subspace.

To obtain the characteristic equations from the integral equation (2.6), we start by setting $\Lambda_0^* = \{\mathbf{q}_1, \mathbf{q}_2, \mathbf{q}_3\}$, where $\mathbf{q}_1 = 2\pi(1,0)^T$, $\mathbf{q}_2 = 2\pi(0,1)^T$, and $\mathbf{q}_3 = 2\pi(-1,-1)^T$, and decompose the Green's function into three parts following (3.3) - (3.5). To compare with the calculations in Section 3, we make change of variable by setting $x_1' = x_1 + x_2$ and $x_2' = x_2 - x_1$ for the Green's function and replace ε by $\varepsilon/\sqrt{2}$ in the integral equation (2.6). It is clear that functions in $\mathcal{H}_o^s(\partial D_1)$ and $\mathcal{H}_e^s(\partial D_1)$ are odd and even with respect to the x_1' axis. The key observation from the decomposition is that $G_{\Lambda_0^*}(\boldsymbol{\kappa}, \omega; \mathbf{x})$ attains a similar expansion as (3.6) in the new coordinate:

$$\begin{aligned} G_{\Lambda_0^*}(\boldsymbol{\kappa}, \omega; \mathbf{x}) = &\frac{1}{\omega^2 - \kappa_+^2 - \kappa^2}\left(2 + 2\imath\kappa_+ x_1' - (\kappa_+^2 x_1'^2 + b^2 x_2'^2)\right) \\ &+ \frac{1}{\omega^2 - 2\kappa_-^2}\left(1 + \imath\kappa_- x_1' - \frac{1}{2}\kappa_-^2 x_1'^2\right) + G_{\Lambda_0^*}^{\infty}(\boldsymbol{\kappa}, \omega; \mathbf{x}'), \end{aligned}$$

where $\kappa_\pm := \kappa \pm 2\pi$. Therefore, by repeating the decomposition of the operators $\mathcal{A}_o$ and $\mathcal{A}_e$ in the function space $\mathcal{H}_o^s(\partial D_1)$ and $\mathcal{H}_e^s(\partial D_1)$ respectively as in Section 3.3, one reduces each subsystem (3.2) into the characteristic equations in the form of (3.19a) - (3.19b). Solving the characteristic equations give two branches of eigenvalues $\omega_o(\kappa)$ and $\omega_e(\kappa)$:

$$\begin{aligned} &\omega_o^2(\kappa) = \kappa_+^2 + \kappa^2 + 2\pi b^2\varepsilon^2\left(1 + O(\varepsilon)\right), \\ &\omega_e^2(\kappa) = 2\kappa_-^2 = \kappa_+^2 + \kappa^2 + 64\pi^4\varepsilon^2\left(1 + O(\varepsilon^2\ln\varepsilon)\right) \text{ for } \kappa = \underline{\kappa} = \frac{\pi}{3} - \frac{16}{3}\pi^3\varepsilon^2 + O(\varepsilon^3\ln\varepsilon), \\ &\omega_e^2(\kappa) = \kappa_+^2 + \kappa^2 = 2\kappa_-^2 + 32\pi^4\varepsilon^2\left(1 + O(\varepsilon^2\ln\varepsilon)\right) \text{ for } \kappa = \bar{\kappa} = \frac{\pi}{3} + \frac{8}{3}\pi^3\varepsilon^2 + O(\varepsilon^3\ln\varepsilon). \end{aligned}$$

In particular, there holds $\omega_o(\underline{\kappa}) - \omega_e(\underline{\kappa}) < 0$ and $\omega_o(\bar{\kappa}) - \omega_e(\bar{\kappa}) > 0$ for sufficiently small ε. We deduce that there exists $\kappa^* \in (\underline{\kappa}, \bar{\kappa})$ such that $\omega_o(\kappa^*) = \omega_e(\kappa^*) = \omega^*$.

THEOREM 4.1. *There exists $\boldsymbol{\kappa}^* = (\kappa^*, \kappa^*)$ as a characteristic value of (2.6), with $\kappa^* \in (\underline{\kappa}, \bar{\kappa})$ satisfying $\omega_o(\kappa^*) = \omega_e(\kappa^*) = \omega^*$. The corresponding eigenspace is span$\{\phi_o, \phi_e\}$, wherein $\phi_o(\mathbf{x}) \in \mathcal{H}_o^{-1/2}(\partial D_1)$ and $\phi_e(\mathbf{x}) \in \mathcal{H}_e^{-1/2}(\partial D_1)$.*

The conical singularity for the dispersion surface near $(\boldsymbol{\kappa}^*, \omega^*)$ can be established in the same way as Section 3.6, and we omit here for conciseness.

4.2. Dirac point on XM. We consider $\boldsymbol{\kappa} = (\pi, \kappa) \in XM$. First, we obtain a decomposition of the Green's function as (3.3) - (3.5) by setting $\Lambda_0^* = \{\mathbf{q}_1, \mathbf{q}_2, \mathbf{q}_3, \mathbf{q}_4\}$, where $\mathbf{q}_1 = 2\pi(0,1)^T$, $\mathbf{q}_2 = 2\pi(0,-1)^T$, $\mathbf{q}_3 = 2\pi(-1,-1)^T$, and $\mathbf{q}_4 = 2\pi(-1,1)^T$.

Again, to compare with the calculations in Section 3, we make change of variables $x_1' = x_2$ and $x_2' = x_1$. Then in the new coordinate, $G_{\Lambda_0^*}$ takes the following form:

$$G_{\Lambda_0^*}(\boldsymbol{\kappa}, \omega; \mathbf{x}') = \frac{1}{\omega^2 - \kappa_+^2 - \pi^2}\left(2 + 2\imath\kappa_+ x_1' - (\kappa_+^2 x_1'^2 + \pi^2 x_2'^2)\right) + \frac{1}{\omega^2 - \kappa_-^2 - \pi^2}\left(1 + 2\imath\kappa_- x_1' - (\kappa_-^2 x_1'^2 + \pi^2 x_2'^2)\right) + G^{\infty}_{\Lambda_0^*}(\boldsymbol{\kappa}, \omega; \mathbf{x}').$$

By restricting the integral operator $\mathcal{S}_\varepsilon^{\boldsymbol{\kappa},\omega}$ onto the subspaces $\mathcal{H}_o^s(\partial D_1)$ and $\mathcal{H}_e^s(\partial D_1)$ that consists of odd and even functions with respect to the x_1' axis, and decomposing the operator $\mathcal{A}_o$ and $\mathcal{A}_e$ as in Section 3.3, we still obtain the characteristic equations in the form of (3.19a) - (3.19b). More explicitly, (3.19a) and (3.19b) now read

$$\begin{aligned}
&\frac{2\pi^3\varepsilon^2}{\omega^2 - \kappa_+^2 - \pi^2} + \frac{2\pi^3\varepsilon^2}{\omega^2 - \kappa_-^2 - \pi^2} - \frac{1}{2} + O(\varepsilon) = 0.\\
&\left((\omega^2 - \kappa_+^2 - \pi^2) + (\omega^2 - \kappa_-^2 - \pi^2)\right)\cdot\left(2 + O\left(\varepsilon^2 \ln\varepsilon\right)\right) - 128\pi^4\varepsilon^2\\
&+ \left(\frac{\ln\varepsilon}{2\pi} + \beta + O(\varepsilon)\right)\cdot(\omega^2 - \kappa_-^2 - \pi^2)\cdot(\omega^2 - \kappa_+^2 - \pi^2) = 0.
\end{aligned}$$

Solving the first equation yields two roots $\omega_o^{\pm}(\kappa)$ satisfying

$$(\omega_o^{\pm}(\kappa))^2 = \kappa_\pm^2 + \pi^2 + 4\rho(\kappa)\pi^3\varepsilon^2\left(1 + O(\varepsilon)\right), \quad \rho(\kappa) \in [\frac{1}{2}, 1].$$

On the other hand, the second equation attains $\omega_e(\kappa)$ that satisfies

$$\begin{aligned}
&\omega_e^2(\kappa) = \kappa_-^2 + \pi^2 = \kappa_+^2 + 128\pi^4\varepsilon^2\left(1 + O(\varepsilon^2\ln\varepsilon)\right) \text{ for } \kappa = \underline{\kappa} = -16\pi^3\varepsilon^2 + O(\varepsilon^3\ln\varepsilon),\\
&\omega_e^2(\kappa) = \kappa_+^2 = \kappa_-^2 + \pi^2 + 128\pi^4\varepsilon^2\left(1 + O(\varepsilon^2\ln\varepsilon)\right) \text{ for } \kappa = \bar{\kappa} = 16\pi^3\varepsilon^2 + O(\varepsilon^3\ln\varepsilon).
\end{aligned}$$

Thus for sufficiently small ε, there holds

$$\begin{aligned}
&\omega_o^-(\underline{\kappa}) - \omega_e(\underline{\kappa}) > 0, \quad \omega_o^-(\bar{\kappa}) - \omega_e(\bar{\kappa}) < 0;\\
&\omega_o^+(\underline{\kappa}) - \omega_e(\underline{\kappa}) < 0, \quad \omega_o^+(\bar{\kappa}) - \omega_e(\bar{\kappa}) > 0.
\end{aligned}$$

We conclude that there exists $\kappa^{*,\pm} \in (\underline{\kappa}, \bar{\kappa})$ such that $\omega_o^{\pm}(\kappa^{*,\pm}) = \omega_e(\kappa^{*,\pm}) = \omega^{*,\pm}$.

THEOREM 4.2. *There exists $\boldsymbol{\kappa}^* = (\pi, \kappa^*)$ as a characteristic value of (2.6), with $\kappa^* \in (\underline{\kappa}, \bar{\kappa})$, and the corresponding eigenspace is span$\{\phi_o, \phi_e\}$, wherein $\phi_o(\mathbf{x})$ and $\phi_e(\mathbf{x})$ is odd and even with respect to the x_2 axis respectively.*

The conical singularity for the dispersion surface near $(\boldsymbol{\kappa}^*, \omega^*)$ can be established similarly.

REMARK 4.3. *Theorems 3.15, 4.1, and 4.2 prove the existence of the Dirac point for some $\boldsymbol{\kappa}^*$ on the boundary of the reduced Brillouin zone ΓXM for the lower spectral bands, or more precisely, the first six spectral bands. Following the same procedure, one can obtain the Dirac point in higher bands, for which the finite-term $G_{\Lambda_0^*}(\boldsymbol{\kappa}, \omega; \mathbf{x}')$ in the decomposition of the Green's function will contain more modes.*

5. Inverse design of Dirac points. Given a pair $(\boldsymbol{\kappa}^*, \omega^*)$, with $\boldsymbol{\kappa}^*$ on the boundary of the reduced Brillouin zone ΓMX, we would like to solve for a dielectric function $\rho(\mathbf{x})$ in (1.2a) such that the spectrum of the differential operator attains a Dirac point at $(\boldsymbol{\kappa}^*, \omega^*)$. The challenge of the computational design lies in achieving two goals simultaneously: the degeneracy at $(\boldsymbol{\kappa}^*, \omega^*)$ and the conical shape of

dispersion surfaces near $(\boldsymbol{\kappa}^*, \omega^*)$. In particular, the enforcement of nonzero slope value at the Dirac point is difficult to impose directly. Based on the analysis of the parity of the Bloch modes at and near a Dirac point in Sections 3 and 4, we apply the local density-of-state (LDOS) method to impose the constraint for the parity of eigenfunctions to solve the inverse design problem.

5.1. The local density-of-state (LDOS) method. In view of Theorems 3.15, 4.1, 4.2, we observe that at a Dirac point, the eigenspace of the integral operator $\mathcal{S}$ attains a two-dimensional eigenspace $span\{\phi_o, \phi_e\}$, wherein $\phi_o(\mathbf{x}) \in \mathcal{H}_o^{-1/2}(\partial D_1)$ and $\phi_e(\mathbf{x}) \in \mathcal{H}_e^{-1/2}(\partial D_1)$.[1] It can be deduced that the corresponding eigenspace for the differential operator in (1.2a) is spanned by $\psi_o(\mathbf{x}) \in \mathcal{H}_o(Y)$ and $\psi_e(\mathbf{x}) \in \mathcal{H}_e(Y)$, which are odd and even in the periodic cell Y along the symmetry axis. Furthermore, from Remark 3.16, the parity of the eigenfunctions corresponding to the two frequency bands crossed at the Dirac point swaps before and after the degeneracy. Therefore, we solve the inverse design problem by finding $\rho(\mathbf{x})$ such that there exist two frequency bands $\omega_m(\boldsymbol{\kappa}) \le \omega_{m+1}(\boldsymbol{\kappa})$ satisfying $\omega_m(\boldsymbol{\kappa}^*) = \omega_{m+1}(\boldsymbol{\kappa}^*)$ and the corresponding Bloch modes $\psi_m(\boldsymbol{\kappa}, \omega; \mathbf{x})$ and $\psi_{m+1}(\boldsymbol{\kappa}, \omega; \mathbf{x})$ satisfy the following:

(G1) The two-dimensional eigenspace $\mathcal{E}_{\boldsymbol{\kappa}^*, \omega^*}$ corresponding to the crossing of the m-th and $m+1$-th dispersion surfaces is spanned by an eigenfunction in $\mathcal{H}_o(Y)$ and an eigenfunction in $\mathcal{H}_e(Y)$.

(G2) The parity of the Bloch modes $\psi_m(\boldsymbol{\kappa}, \omega; \mathbf{x})$ and $\psi_{m+1}(\boldsymbol{\kappa}, \omega; \mathbf{x})$ swaps before and after the crossing of $\omega_m(\boldsymbol{\kappa})$ and $\omega_{m+1}(\boldsymbol{\kappa})$ at $(\boldsymbol{\kappa}^*, \omega^*)$. That is, on one side of the crossing, $\psi_m(\boldsymbol{\kappa}, \omega; \mathbf{x}) \in \mathcal{H}_o(Y)$ and $\psi_{m+1}(\boldsymbol{\kappa}, \omega; \mathbf{x}) \in \mathcal{H}_e(Y)$ and visa versa on the other side of the crossing.

To treat the boundary condition more conveniently, we express the Bloch mode in (1.2a) as $\psi(\boldsymbol{\kappa}, \omega; \mathbf{x}) = e^{\imath \boldsymbol{\kappa} \cdot \mathbf{x}} \phi(\boldsymbol{\kappa}, \omega; \mathbf{x})$, wherein the periodic function $\phi(\boldsymbol{\kappa}, \omega; \mathbf{x})$ satisfies

$$(\nabla + \imath\boldsymbol{\kappa}) \cdot (\nabla + \imath\boldsymbol{\kappa}) \phi(\boldsymbol{\kappa}, \omega; \mathbf{x}) + \omega^2 \rho(\mathbf{x}) \phi(\boldsymbol{\kappa}, \omega; \mathbf{x}) = 0 \qquad \mathbf{x} \in \mathbb{R}^2 \tag{5.1a}$$

$$\phi(\boldsymbol{\kappa}, \omega; \mathbf{x} + \mathbf{e}) = \phi(\boldsymbol{\kappa}, \omega; \mathbf{x}) \qquad \mathbf{e} \in \Lambda. \tag{5.1b}$$

Let $\langle \phi, \psi \rangle = \displaystyle\int_Y \phi(\mathbf{x}) \overline{\psi(\mathbf{x})}\, d\mathbf{x}$, we define the Hilbert spaces of periodic functions

$$\mathcal{L}^2_{\rho,p}(Y) := \{\phi(\mathbf{x}) \colon \ \langle \rho\phi, \phi \rangle < \infty, \phi(\mathbf{x} + \mathbf{e}) = \phi(\mathbf{x}),\ \forall \mathbf{e} \in \Lambda\},$$
$$\mathcal{H}^1_{\rho,p}(Y) := \{\phi(\mathbf{x}) \in \mathcal{L}^2_{\rho,p}(Y) \colon \ \partial_i \phi(\mathbf{x}) \in \mathcal{L}^2_{\rho,p}(Y),\ i = 1, 2\}.$$

To achieve band degeneracy at $(\boldsymbol{\kappa}^*, \omega^*)$ with the Bloch modes satisfying the above parity, we seek to maximize the local density-of-state (LDOS) radiated by dipoles arranged at proper locations [19]. Let u be the periodic part of the wave field radiated by a collection of dipoles $s(\mathbf{x}) = \sum_{j=1}^J \alpha_j \delta(\mathbf{x} - \mathbf{y}_j)$ that solves

$$(\nabla + \imath\boldsymbol{\kappa}) \cdot (\nabla + \imath\boldsymbol{\kappa}) u(\boldsymbol{\kappa}, \omega; \mathbf{x}) + \omega^2 \rho(\mathbf{x}) u(\boldsymbol{\kappa}, \omega; \mathbf{x}) = -\imath\omega e^{-\imath \boldsymbol{\kappa} \cdot x} s(\mathbf{x}) \quad \text{in } Y, \tag{5.2}$$

the local density of eigenstates is defined by (cf. [19])

$$\mathrm{LDOS}(\boldsymbol{\kappa}, \omega) := -\frac{6}{\pi} \mathrm{Re} \left\{ \int_Y u(\boldsymbol{\kappa}, \omega; \mathbf{x}) e^{\imath \boldsymbol{\kappa} \cdot x} \overline{s(\mathbf{x})}\, d\mathbf{x} \right\}. \tag{5.3}$$

[1] For $\boldsymbol{\kappa}$ located on ΓM, XM and ΓX, the axis of symmetry is x_1, x_2 and $x_1 x_2$ respectively for functions in $\mathcal{H}_o^{-1/2}(\partial D_1)$ and $\mathcal{H}_e^{-1/2}(\partial D_1)$.

To attain an eigenvalue at $(\boldsymbol{\kappa}^*, \omega^*)$, one maximizes the following frequency-averaged local density-of-eigenstate function:

$$L_s(\boldsymbol{\kappa}^*, \omega^*) = \int_{-\infty}^{\infty} \mathrm{LDOS}(\boldsymbol{\kappa}^*, \omega) W(\omega^*; \omega)\, d\omega, \tag{5.4}$$

in which $W(\omega^*; \omega)$ is a window function peaked at a desired frequency ω^*. The desired parity for eigenfunctions specified in (G1)(G2) above is achieved by choosing the amplitude α_j and the dipole locations $\mathbf{y}_j$ suitably. For instance, two dipoles placed with mirror symmetry along the symmetry axis and $\alpha_1 = \alpha_2$ give rises to even parity for the eigenfunction, while two dipoles at the same locations with $\alpha_1 = -\alpha_2$ yield odd parity for the eigenfunction.

5.2. Slope of the dispersion surface. Assume that $(\boldsymbol{\kappa}^*, \omega^*)$ is a Dirac point. Let us express the dispersion surface near $(\boldsymbol{\kappa}^*, \omega^*)$ as $\boldsymbol{\kappa} = \boldsymbol{\kappa}^* + \delta\boldsymbol{\kappa}$ and $\omega = \omega^* + \delta\omega$, and the periodic eigenfunction as $\phi = \phi^* + \delta\phi$. Then it can be shown that $\delta\phi$ satisfies

$$(\nabla + \imath\boldsymbol{\kappa}) \cdot (\nabla + \imath\boldsymbol{\kappa})\delta\phi(\mathbf{x}) + \omega^2 \rho(\mathbf{x})\delta\phi(\mathbf{x}) = F(\mathbf{x}) \quad \mathbf{x} \in Y,$$

where

$$F(\mathbf{x}) = -2\delta\omega\, \omega^* \phi^* - 2\imath\delta\boldsymbol{\kappa} \cdot (\nabla + \imath\boldsymbol{\kappa}^*)\phi^* + O(|\delta\boldsymbol{\kappa}|^2, |\delta\omega|^2). \tag{5.5}$$

From the Fredholm alternative and neglecting the high-order terms in $F(\mathbf{x})$, we obtain

$$\langle \delta\omega\, \omega^* \phi^* + \imath\delta\boldsymbol{\kappa} \cdot (\nabla + \imath\boldsymbol{\kappa}^*)\phi^*, \phi_j \rangle = 0, \quad j = o, e. \tag{5.6}$$

Expanding ϕ^* as $\phi^* = \alpha_o \phi_o + \alpha_e \phi_e$, (5.6) is cast as the following linear system:

$$\begin{pmatrix} \delta\omega\, \omega^* + \imath\delta\boldsymbol{\kappa} \cdot \langle (\nabla + \imath\boldsymbol{\kappa}^*)\phi_o, \phi_o \rangle & \imath\delta\boldsymbol{\kappa} \cdot \langle (\nabla + \imath\boldsymbol{\kappa}^*)\phi_e, \phi_o \rangle \\ \imath\delta\boldsymbol{\kappa} \cdot \langle (\nabla + \imath\boldsymbol{\kappa}^*)\phi_o, \phi_e \rangle) & \delta\omega\, \omega^* + \imath\delta\boldsymbol{\kappa} \cdot \langle (\nabla + \imath\boldsymbol{\kappa}^*)\phi_e, \phi_e \rangle \end{pmatrix} \begin{pmatrix} \alpha_o \\ \alpha_e \end{pmatrix} = \begin{pmatrix} 0 \\ 0 \end{pmatrix}.$$

Denote the above 2×2 matrix as $\mathcal{M}(\delta\boldsymbol{\kappa}, \delta\omega)$, then the leading-order of the dispersion relation is expressed by the equation $\det \mathcal{M}(\delta\boldsymbol{\kappa}, \delta\omega) = 0$.

For $\boldsymbol{\kappa}^*$ on the boundary of the reduced Brillouin zone, we express $\boldsymbol{\kappa}^*$ as $\boldsymbol{\kappa}^* = \kappa_1^* \mathbf{p}_1 + \kappa_2^* \mathbf{p}_2$ with the unit vector $\mathbf{p}_1$ given by $\mathbf{e}_1$, $\mathbf{e}_2$, and $(\mathbf{e}_1 + \mathbf{e}_2)/\sqrt{2}$ respectively when $\boldsymbol{\kappa}^*$ is on ΓX, XM and ΓM respectively [2]. Let $\mathbf{p}_2$ be the unit vector such that $\mathbf{p}_1 \cdot \mathbf{p}_2 = 0$. Correspondingly, we write $\delta\boldsymbol{\kappa}$ as $\delta\boldsymbol{\kappa} = \delta\kappa_1 \mathbf{p}_1 + \delta\kappa_2 \mathbf{p}_2$. Note that, from the symmetry of Bloch modes, there holds

$$\begin{aligned} &\langle \phi_o, \phi_e \rangle = 0, \quad \left\langle \partial_{\mathbf{p}_2}(e^{\imath\boldsymbol{\kappa}^* \cdot x}\phi_j), e^{\imath\boldsymbol{\kappa}^* \cdot x}\phi_j \right\rangle = 0, \quad j = o \text{ or } e, \\ &\mathrm{Re}\, \langle \partial_{\mathbf{p}_1}\phi_j, \phi_j \rangle = 0, \quad \langle \partial_{\mathbf{p}_i}\phi_j, \phi_k \rangle = -\overline{\langle \partial_{\mathbf{p}_i}\phi_k, \phi_j \rangle}, \quad j, k = o \text{ or } e, \end{aligned}$$

where the partial derivative $\partial_{\mathbf{p}_j}$ is taken with respect to the spatial variable $\mathbf{x}$. As such the matrix A reduces to

$$\begin{pmatrix} \delta\omega\, \omega^* - \delta\kappa_1 \left(\mathrm{Im}\langle \partial_{\mathbf{p}_1}\phi_o, \phi_o \rangle + \kappa_1^* \langle \phi_o, \phi_o \rangle\right) & \overline{\imath\delta\boldsymbol{\kappa} \cdot \langle \nabla\phi_o, \phi_e \rangle} \\ \imath\delta\boldsymbol{\kappa} \cdot \langle \nabla\phi_o, \phi_e \rangle & \delta\omega\, \omega^* - \delta\kappa_1 \left(\mathrm{Im}\langle \partial_{\mathbf{p}_1}\phi_e, \phi_e \rangle + \kappa_1^* \langle \phi_e, \phi_e \rangle\right) \end{pmatrix}.$$

[2] The choice of $\mathbf{p}_1$ is not unique when $\boldsymbol{\kappa}$ is located on the vertices Γ, M, or X. We use either of the two specified vectors.

Therefore, the dispersion relation near the Dirac point $(\boldsymbol{\kappa}^*, \omega^*)$ is given by

$$\det \mathcal{M} = \Big(\omega^*\,\delta\omega - \mu_1^{(o)}\delta\kappa_1\Big)\cdot\Big(\omega^*\,\delta\omega - \mu_1^{(e)}\delta\kappa_1\Big) - |\mu_1^{(o,e)}\delta\kappa_1 + \mu_2^{(o,e)}\delta\kappa_2|^2 = 0,$$

where

$$\begin{aligned} &\mu_1^{(o,o)} = \mathrm{Im}\langle\partial_{\mathbf{p}_1}\phi_o, \phi_o\rangle + \kappa_1^*\langle\phi_o, \phi_o\rangle, \quad \mu_1^{(e,e)} = \mathrm{Im}\langle\partial_{\mathbf{p}_1}\phi_e, \phi_e\rangle + \kappa_1^*\langle\phi_e, \phi_e\rangle, \\ &\mu_1^{(o,e)} = \langle\partial_{\mathbf{p}_1}\phi_o, \phi_e\rangle, \quad \mu_2^{(o,e)} = \langle\partial_{\mathbf{p}_2}\phi_o, \phi_e\rangle. \end{aligned} \tag{5.7}$$

By rewriting the above equation as

$$\big(\omega^*\,\delta\omega - \mu_1^+\delta\kappa_1\big)^2 - (\mu_1^-)^2(\delta\kappa_1)^2 - |\mu_1^{(o,e)}\delta\kappa_1 + \mu_2^{(o,e)}\delta\kappa_2|^2 = 0,$$

with $\mu_1^{\pm} = \frac{\mu_1^{(o)} \pm \mu_1^{(e)}}{2}$, we obtain the dispersion relation near $(\boldsymbol{\kappa}^*, \omega^*)$ as

$$\omega(\boldsymbol{\kappa}) = \omega^* + \frac{\mu_\pm(\bar{\boldsymbol{\kappa}})}{\omega^*}|\boldsymbol{\kappa} - \boldsymbol{\kappa}^*| + O(|\boldsymbol{\kappa} - \boldsymbol{\kappa}^*|^2), \tag{5.8}$$

wherein

$$\mu_\pm(\bar{\boldsymbol{\kappa}}) = \mu_1^+(\bar{\boldsymbol{\kappa}}\cdot\mathbf{p}_1) \pm \sqrt{(\mu_1^-)^2(\bar{\boldsymbol{\kappa}}\cdot\mathbf{p}_1)^2 + |\mu_1^{(o,e)}(\bar{\boldsymbol{\kappa}}\cdot\mathbf{p}_1) + \mu_2^{(o,e)}(\bar{\boldsymbol{\kappa}}\cdot\mathbf{p}_2)|^2} \tag{5.9}$$

for $\bar{\boldsymbol{\kappa}} = \frac{\delta\boldsymbol{\kappa}}{\|\delta\boldsymbol{\kappa}\|}$.

REMARK 5.1. *We will enforce "the nontrivial slope values $\mu_\pm(\bar{\boldsymbol{\kappa}})$" constraint in the optimization framework below when generating a pair of Dirac cones at $(\boldsymbol{\kappa}^*, \omega^*)$. From various numerical examples in Section 5.5, it is observed that one can achieve $|\mu_\pm(\bar{\boldsymbol{\kappa}})| > 0$ on the boundary of the reduced Brillouin zone ΓXM that excludes the vertices Γ, X, and M. The absence of Dirac points at Γ, X, and M is attributed to the reflection symmetry imposed for the Bloch modes. For example, $\boldsymbol{\kappa}^* = X$ can be viewed as a Bloch wave vector on ΓX or XM, then (G1) implies that the Bloch mode ψ is even/odd with respect to both horizontal and vertical axes, and a direct calculation using (5.7) leads to $\mu_\pm(\mathbf{p}_1) = \mu_\pm(\mathbf{p}_2) = 0$. We recall the absence of the Dirac point for $\boldsymbol{\kappa}^* = M$ proved in [14], wherein the slope of the dispersion surfaces vanishes when the two Bloch modes at the degeneracy point $(\boldsymbol{\kappa}^*, \omega^*)$ attain different rotation symmetry. Mathematically, it will be interesting to investigate what Bloch modes will give rise to a linear dispersion relation at the vertices Γ, X, and M.*

5.3. The optimization framework. Our inverse design consists of two steps. In the first step, we aim to design a periodic medium to achieve a degeneracy point at the desired location $(\boldsymbol{\kappa}^*, \omega^*)$ such that the two Bloch modes at and near $(\boldsymbol{\kappa}^*, \omega^*)$ satisfy (G1)(G2). Following the discussions in Section 5.1, we choose $\boldsymbol{\kappa}_\pm^* = \boldsymbol{\kappa}^* \pm \Delta\kappa\cdot\mathbf{p}_1$, $\omega_\pm^* = \omega^* \pm \Delta\omega$ with small $\Delta\kappa$ and $\Delta\omega$ and propose the optimization framework in the following form:

$$\max_{\underline{\rho}\le\rho\le\overline{\rho}} \min\Big\{L_{s_i}(\boldsymbol{\kappa}, \omega);\ i = o, e,\ (\boldsymbol{\kappa}, \omega) \in \{(\boldsymbol{\kappa}^*, \omega^*), (\boldsymbol{\kappa}_\pm^*, \omega_\pm^*)\}\Big\}, \tag{5.10}$$

where L_{s_i} is the LDOS functions (5.4) with the chosen source functions $s_i(\mathbf{x})$ in the form of (5.2) to achieve the desired parity for eigenfunctions. To solve the problem efficiently, we may reformulate the maxmin problem (5.10) as a constrained optimization problem as follows and apply the quasi-Newton method. Let

$$F_j(\rho) = -L_{s_i}(\boldsymbol{\kappa}, \omega) \quad (j = 1, \cdots, 6)$$

be the opposite of the six LDOS functions with $i = o, e$ and $(\boldsymbol{\kappa}, \omega) \in \{(\boldsymbol{\kappa}^*, \omega^*), (\boldsymbol{\kappa}^*_\pm, \omega^*_\pm)$ in (5.10). Then the maxmin problem (5.10) is equivalent to the constrained optimization problem:

$$\begin{aligned} &\min_{\underline{\rho} \le \rho \le \overline{\rho}} \ \theta \\ &F_j(\rho) \le \theta, \quad j = 1, 2, \cdots, 6. \end{aligned} \tag{5.11}$$

In the second step, we impose the constraint on the slope of the dispersion surface so that its value is nontrivial. To this end, we impose the condition

$$|\mu_\pm(\mathbf{p}_1)|^2 \ge \sigma \quad \text{and} \quad |\mu_\pm(\mathbf{p}_2)|^2 \ge \sigma$$

for some positive constant σ, where $\mu_\pm(\bar{\boldsymbol{\kappa}})$ is defined in (5.9). Correspondingly, we propose the following optimization framework:

$$\begin{aligned} &\min_{\underline{\rho} \le \rho \le \overline{\rho}} \ \theta - \lambda\sigma \\ &F_j(\rho) \le \theta, \quad j = 1, 2, \cdots, 6; \\ &\sigma \le |\mu_\pm(\mathbf{p}_j)|^2, \quad j = 1, 2. \end{aligned} \tag{5.12}$$

In the above, $\lambda > 0$ as a penalization parameter.

5.4. Implementation details. The optimization problems in (5.11) and (5.12) are numerically solved using a gradient-based, BFGS quasi-Newton method where the constraints are enforced using an interior-point strategy, as implemented in Matlab's `fmincon` function. The gradients of F_j and $|\mu_\pm(\mathbf{p}_j)|^2$, $j = 1, 2$ are provided below in Theorem 5.2 and Theorem 5.4, respectively.

5.4.1. The computation of the LDOS function and the Fréchet derivative. We choose the window function $W(\omega^*; \omega) = \frac{2\gamma^3/\pi}{((\omega-\omega^*)+\gamma^2)^2}$, which is a normalized square of a Lorentzian function peaked at ω^* with the band width γ. By the residue theorem, it can be calculated that the frequency-averaged LDOS defined in (5.4) can be evaluated at a single complex frequency $\tilde{\omega}^* := \omega^* + \imath\gamma$ and there holds (cf. [19]))

$$L_s(\boldsymbol{\kappa}^*, \omega^*) = \mathrm{Re}\Big(L(\boldsymbol{\kappa}^*, \tilde{\omega}^*) - \imath\gamma\partial_\omega L(\boldsymbol{\kappa}^*, \tilde{\omega}^*)\Big), \tag{5.13}$$

where $L(\boldsymbol{\kappa}, \omega) = -\dfrac{6}{\pi}\displaystyle\int_Y u(\boldsymbol{\kappa}, \omega; \mathbf{x}) e^{\imath\boldsymbol{\kappa}\cdot x}\, \overline{s(\mathbf{x})}\, d\mathbf{x}$. To compute $\partial_\omega L(\boldsymbol{\kappa}, \omega)$, we introduce the adjoint problem

$$\begin{aligned} &(\nabla - \imath\boldsymbol{\kappa}) \cdot (\nabla - \imath\boldsymbol{\kappa}) v(\boldsymbol{\kappa}, \omega; \mathbf{x}) + \omega^2 \rho(\mathbf{x}) v(\boldsymbol{\kappa}, \omega; \mathbf{x}) = -\imath\omega e^{\imath\boldsymbol{\kappa}\cdot x}\overline{s(\mathbf{x})} \quad && \mathbf{x} \in \mathbb{R}^2, \\ &v(\boldsymbol{\kappa}, \omega; \mathbf{x} + \mathbf{e}) = v(\boldsymbol{\kappa}, \omega; \mathbf{x}) && \mathbf{e} \in \Lambda. \end{aligned} \tag{5.14}$$

Then

$$\partial_\omega L(\boldsymbol{\kappa}, \omega) = -\frac{6}{\pi\omega}\int_Y v(\boldsymbol{\kappa}, \omega; \mathbf{x})\, s(\mathbf{x})\, d\mathbf{x} + \frac{12\imath}{\pi}\int_Y \rho(\mathbf{x}) u(\boldsymbol{\kappa}, \omega; \mathbf{x}) v(\boldsymbol{\kappa}, \omega; \mathbf{x})\, d\mathbf{x}. \tag{5.15}$$

THEOREM 5.2. *$L_s(\boldsymbol{\kappa}^*, \omega^*)$ is Fréchet differentiable with respect to $\rho(\mathbf{x})$. Let δL_s be the perturbation of $L_s(\boldsymbol{\kappa}^*, \omega^*)$ when $\rho(\mathbf{x})$ is perturbed by $\delta\rho(\mathbf{x})$, then*

$$\delta L_s(\boldsymbol{\kappa}^*, \omega^*) = Re \int_Y \delta\rho(\mathbf{x}) g(\mathbf{x})\, d\mathbf{x} + O\left(\|\delta\rho\|^2\right), \tag{5.16}$$

where

$$g(\mathbf{x}) = \frac{6}{\pi}(\imath\omega^* + 2\gamma)\, u(\boldsymbol{\kappa}^*, \tilde{\omega}^*; \mathbf{x}) v(\boldsymbol{\kappa}^*, \tilde{\omega}^*; \mathbf{x}) + \frac{12\gamma}{\pi}(\omega^* + \imath\gamma)^2 \Big(u(\boldsymbol{\kappa}^*, \tilde{\omega}^*; \mathbf{x}) w_1(\boldsymbol{\kappa}^*, \tilde{\omega}^*; \mathbf{x}) + u(\boldsymbol{\kappa}^*, \tilde{\omega}^*; \mathbf{x}) w_2(\boldsymbol{\kappa}^*, \tilde{\omega}^*; \mathbf{x}) \Big).$$

In the above, $w_1(\boldsymbol{\kappa}, \omega; \mathbf{x})$ *and* $w_2(\boldsymbol{\kappa}, \omega; \mathbf{x}) \in \mathcal{H}^1_{\rho,p}(Y)$ *satisfy*

$$(\nabla - \imath\boldsymbol{\kappa}) \cdot (\nabla - \imath\boldsymbol{\kappa}) w_1(\boldsymbol{\kappa}, \omega; \mathbf{x}) + \omega^2 \rho(\mathbf{x}) w_1(\boldsymbol{\kappa}, \omega; \mathbf{x}) = \rho(\mathbf{x}) v(\boldsymbol{\kappa}, \omega; \mathbf{x}), \tag{5.17}$$

$$(\nabla - \imath\boldsymbol{\kappa}) \cdot (\nabla - \imath\boldsymbol{\kappa}) w_2(\boldsymbol{\kappa}, \omega; \mathbf{x}) + \omega^2 \rho(\mathbf{x}) w_2(\boldsymbol{\kappa}, \omega; \mathbf{x}) = \rho(\mathbf{x}) u(\boldsymbol{\kappa}, \omega; \mathbf{x}). \tag{5.18}$$

Proof. A direct perturbation of (5.13) and (5.15) yields

$$\begin{aligned} \delta L_s = &-\frac{6}{\pi}\int_Y \delta u(\mathbf{x})\, s(\mathbf{x})\, d\mathbf{x} + \frac{6\imath\gamma}{\pi\omega}\int_Y \delta v(\mathbf{x})\, s(\mathbf{x})\, d\mathbf{x} \\ &+ \frac{12\gamma}{\pi}\int_Y \delta\rho(\mathbf{x}) u(\mathbf{x}) v(\mathbf{x}) + \rho(\mathbf{x})\delta u(\mathbf{x}) v(\mathbf{x}) + \rho(\mathbf{x}) u(\mathbf{x}) \delta v(\mathbf{x})\, d\mathbf{x}. \end{aligned} \tag{5.19}$$

In view of (5.2) and (5.14), $\delta u(\mathbf{x})$ and $\delta v(\mathbf{x})$ satisfy

$$\begin{aligned} &(\nabla + \imath\boldsymbol{\kappa}) \cdot (\nabla + \imath\boldsymbol{\kappa}) \delta u(\mathbf{x}) + \omega^2 \rho(\mathbf{x}) \delta u(\mathbf{x}) = -\omega^2 \delta\rho(\mathbf{x}) u(\mathbf{x}); \\ &(\nabla - \imath\boldsymbol{\kappa}) \cdot (\nabla - \imath\boldsymbol{\kappa}) \delta v(\mathbf{x}) + \omega^2 \rho(\mathbf{x}) \delta v(\mathbf{x}) = -\omega^2 \delta\rho(\mathbf{x}) v(\mathbf{x}). \end{aligned}$$

The desired formula for $g(\mathbf{x})$ is obtained by applying the Green's second identity to each pair $(v, \delta u)$, $(u, \delta v)$, $(\delta u, w_1)$ and $(\delta v, w_2)$, and substituting into (5.19). ∎

5.4.2. The Fréchet derivative of slope functions. In view of (5.9), the Fréchet derivative of slope functions with respect to $\rho(\mathbf{x})$ boils down to the Fréchet derivative of $\mu_1^{(i,j)}$ and $\mu_2^{(i,j)}$ for $i, j = o, e$, which is obtained in what follows.

First, let $\phi_i \in \mathcal{H}^1_{\rho,p}(Y)$ $(i = o, e)$ be an eigenfunction at $\boldsymbol{\kappa} = \boldsymbol{\kappa}^*$ with norm $\|\phi_i\|_{\mathcal{L}^2_{\rho,p}(Y)} = 1$ that satisfies (5.1a). Assume that ρ is perturbed by $\delta\rho$, then the perturbation of the eigenfunction satisfies

$$(\nabla + \imath\boldsymbol{\kappa}^*) \cdot (\nabla + \imath\boldsymbol{\kappa}^*) \delta\phi_i + (\omega^*)^2 \rho \delta\phi_i = -2\omega^* \delta\omega \rho\phi_i - (\omega^*)^2 \delta\rho\phi_i + o(\|\rho\|). \tag{5.20}$$

In the above, the perturbation of the frequency is given by

$$\delta\omega = -\frac{\omega^*}{2}\int_Y \delta\rho(\mathbf{x}) |\phi_i(\mathbf{x})|^2\, d\mathbf{x}, \tag{5.21}$$

which follows from the relation (5.1a), (5.20) and the Green's identity. Furthermore, from $\|\phi_i\|_{\mathcal{L}^2_{\rho,p}(Y)} = \|\phi_i + \delta\phi_i\|_{\mathcal{L}^2_{\rho,p}(Y)} = 1$, it can be deduced that

$$\langle \rho\delta\phi_i, \phi_i \rangle = -\frac{1}{2}\int_Y \delta\rho(\mathbf{x}) |\phi_i(\mathbf{x})|^2\, d\mathbf{x} + \imath\alpha_i \quad \text{for some real number } \alpha_i. \tag{5.22}$$

LEMMA 5.3. *Let* $\delta\phi_i$ *be the perturbation of the eigenfunction that satisfies* (5.20). *For any* $f \in \mathcal{L}^2_{\rho,p}(Y)$, *there holds*

$$\langle \delta\phi_i, f \rangle = -(\omega^*)^2 \int_Y \delta\rho(\mathbf{x}) \phi_i(\mathbf{x}) \overline{v(\mathbf{x})}\, d\mathbf{x} + \imath\alpha_i \langle \phi_i, f \rangle + o(\|\rho\|), \tag{5.23}$$

where α_i *is defined in* (5.22), *and* $v \in \mathcal{H}^1_{\rho,p}(Y)$ *satisfies*

$$(\nabla + \imath\boldsymbol{\kappa}^*) \cdot (\nabla + \imath\boldsymbol{\kappa}^*) v + (\omega^*)^2 \rho v + 2(\omega^*)^2 \rho \langle \rho v, \phi_i \rangle \phi_i = f \quad \text{in } Y. \tag{5.24}$$

The proof of Lemma 5.3 uses the adjoint state method and it is provided in the supplementary materials. Note that we introduce the projection term $2(\omega^*)^2\rho\,\langle \rho v, \phi_i\rangle\,\phi_i$ in (5.24) such that the boundary value problem attains a unique solution in $\mathcal{H}^1_{\rho,p}(Y)$. This is necessary for computational purpose as ω^* is the eigenfrequency that satisfies (5.1a), and the differential operator $(\nabla+\imath\boldsymbol{\kappa}^*)\cdot(\nabla+\imath\boldsymbol{\kappa}^*)+(\omega^*)^2\rho$ attains a nontrivial kernel.

THEOREM 5.4. *Let*

$$J_1(\rho) := \langle \phi_i, \phi_i\rangle, \quad J_2(\rho) := \langle \partial_k\phi_i, \phi_i\rangle \quad J_3(\rho) := \langle \partial_k\phi_o, \phi_e\rangle.$$

Then $J_m(\rho)$ $(m=1,2,3)$ is Fréchet differentiable and there holds

$$\begin{aligned} J_1(\rho+\delta\rho) &= J_1(\rho) + \langle \delta\rho, g_i\rangle + o\left(\|\delta\rho\|\right), \\ J_2(\rho+\delta\rho) &= J_2(\rho) + \langle \delta\rho, g_{ik}\rangle + o\left(\|\delta\rho\|\right), \\ J_3(\rho+\delta\rho) &= J_3(\rho) + \langle \delta\rho, g_{oek}\rangle + \imath\alpha_o\langle\phi_o, \partial_k\phi_e\rangle - \imath\alpha_e\langle\partial_k\phi_o, \phi_e\rangle + o\left(\|\delta\rho\|\right), \end{aligned} \tag{5.25}$$

where

$$\begin{aligned} g_i(\mathbf{x}) &= -2(\omega^*)^2\cdot Re\left\{\phi_i(\mathbf{x})\overline{v_i(\mathbf{x})}\right\}, \\ g_{ik}(\mathbf{x}) &= 2\imath(\omega^*)^2\cdot Im\left\{\phi_i(\mathbf{x})\overline{v_{ik}(\mathbf{x})}\right\}, \\ g_{oek}(\mathbf{x}) &= (\omega^*)^2\cdot\Big(\phi_o(\mathbf{x})\overline{v_{eok}(\mathbf{x})} - \overline{\phi_e(\mathbf{x})}v_{oek}(\mathbf{x})\Big). \end{aligned} \tag{5.26}$$

In the above, v_i, v_{ik}, and v_{ijk} solves (5.24) with $f=\phi_i$, $\partial_k\phi_i$, and $\partial_k\phi_j$, respectively.

Proof. A direct perturbation of $J(\rho)$ yields

$$\begin{aligned} J_1(\rho+\delta\rho) - J_1(\rho) &= 2\mathrm{Re}\langle\delta\phi_i, \phi_i\rangle + o(\|\delta\rho\|) \\ &= -2(\omega^*)^2\cdot\mathrm{Re}\int_Y \delta\rho(\mathbf{x})\phi_i(\mathbf{x})\overline{v_i(\mathbf{x})}\,d\mathbf{x} + o(\|\delta\rho\|). \end{aligned}$$

Similarly,

$$\begin{aligned} J_2(\rho+\delta\rho) - J_2(\rho) &= \langle\partial_k(\delta\phi_i), \phi_i\rangle + \langle\partial_k\phi_i, \delta\phi_i\rangle + o(\|\delta\rho\|) \\ &= -\langle\delta\phi_i, \partial_k\phi_i\rangle + \langle\partial_k\phi_i, \delta\phi_i\rangle + o(\|\delta\rho\|) \\ &= 2\imath(\omega^*)^2\cdot\mathrm{Im}\left\{\int_Y \delta\rho(\mathbf{x})\phi_i(\mathbf{x})\overline{v_{ik}(\mathbf{x})}\,d\mathbf{x}\right\} + o(\|\delta\rho\|), \end{aligned}$$

where we have used the fact that $\mathrm{Re}\langle\phi_i, \partial_k\phi_i\rangle = 0$. The perturbation of $J_3(\rho)$ follows in parallel. ∎

5.5. Numerical examples. In all examples, it is assumed that $1 \le \rho(\mathbf{x}) \le 20$. We discretize the boundary value problem (5.2) and the adjoint problems (5.17), (5.18), (5.24) using the finite element method over a triangular mesh of size $h = 1/n$, as shown in Figure 5.1 (Left). The dielectric function $\rho(\mathbf{x})$ is assumed to be constant over each small square consisting of two small triangles. To generate the Bloch modes ψ_o and ψ_e that satisfy the desired parity specified in (G1)(G2), we choose the dipole sources s_o and s_e in the form of $s_i(\mathbf{x}) = \sum_{j=1}^2 \alpha_{ij}\delta(\mathbf{x}-\mathbf{y}_{ij})$ $(i=o,e)$ such that $\mathbf{y}_{i1}+\mathbf{y}_{i2}$ is located on the symmetry axis. Furthermore, the coefficients α_{ij} satisfy $\alpha_{o1} = -\alpha_{o2} = 1$ and $\alpha_{e1} = \alpha_{e2} = 1$ for the odd and even mode respectively. The last

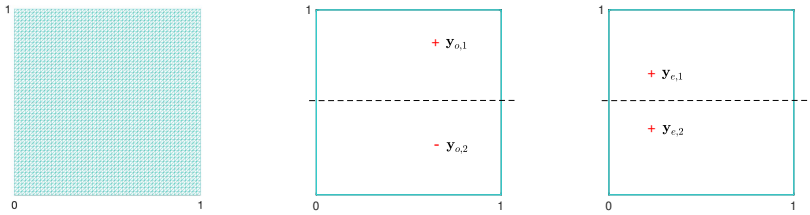

FIG. 5.1. *Left: The triangular mesh used to discretize the PDEs over the unit cell. Middle and Right: The dipole source locations* $\mathbf{y}_{i1}$ *and* $\mathbf{y}_{i2}$ $(i = o, e)$ *when the symmetry axis is horizontal.*

two rows of Tables 5.1-5.2 collect the dipole locations that are used in the numerical computation when $\boldsymbol{\kappa}^*$ is on XM, ΓX and XM respectively. The corresponding LDOS function $L_{s_i}(\boldsymbol{\kappa}, \omega)$ is computed via the formulas (5.13) - (5.15), wherein $u(\mathbf{x})$ and $v(\mathbf{x})$ solves (5.2) and (5.14) respectively with the desired dipole sources $s_i(\mathbf{x})$.

When solving the optimization problems (5.11) and (5.12), for simplicity we start with an initial guess with a constant dielectric function $\rho(\mathbf{x}) \equiv 5$ and set a tolerance value of $\varepsilon = 10^{-5}$ on either the relative change on step size or the objective function value. In each iteration, the gradient for the LDOS functions $L_{s_i}(\boldsymbol{\kappa}, \omega)$ $(i = o, e)$ and the slope functions $\mu_{\pm}(\mathbf{p}_j)$ $(j = 1, 2)$ is computed via (5.16) and (5.25).

The penalization parameter λ in (5.12) is given in second row of Tables 5.1-5.2 for various $\boldsymbol{\kappa}^*$. Figures 5.2, 5.5 and 5.7 demonstrate the Dirac cones that are obtained at the desired $(\boldsymbol{\kappa}^*, \omega^*)$ by solving the optimization problems (5.11) and (5.12) sequentially. Let $\mu^* = \min\{|\mu_{\pm}(\mathbf{p}_1)|, |\mu_{\pm}(\mathbf{p}_2)|\}$ be the minimum of the cone slope value along the directions $\mathbf{p}_1$ and $\mathbf{p}_2$, wherein $\mu_{\pm}(\bar{\boldsymbol{\kappa}})$ is defined in (5.9). The third row of Tables 5.1-5.2 collects the the minimum slope value for each pair of the Dirac cones in Figures 5.2, 5.5 and 5.7. For completeness, we also plot the optimized solution for the dielectric function $\rho(\mathbf{x})$ in Figure 5.3, 5.6 and 5.7. To show the swap the parity of the Bloch mode $\psi(\boldsymbol{\kappa}, \omega; \mathbf{x})$ before and after crossing of the spectral bands at the Dirac point $(\boldsymbol{\kappa}^*, \omega^*)$, in Figure 5.4 we plot the $\psi(\boldsymbol{\kappa}, \omega; \mathbf{x})$ for the second and third band near the Dirac point $(\boldsymbol{\kappa}^*, \omega^*)$ when $\boldsymbol{\kappa}^* = (\pi, 0.3\pi)$ and $\omega^* = 2.0$.

TABLE 5.1

The penalization parameter λ *(second row), the minimum slope value* μ^* *for the Dirac cones (third row), and the dipole sources locations (fourth and fifth row) when* $\boldsymbol{\kappa}^* = (\pi, \kappa^*\pi)$. $\mathbf{x}_c = \frac{1}{2}(\mathbf{e}_1 + \mathbf{e}_2)$ *is the center of the unit cell.*

κ^*	0.1	0.2	0.3	0.4	0.5	0.6	0.7	0.8	0.9
λ	50	50	50	50	100	100	50	50	50
μ^*	0.08	0.16	0.21	0.22	0.23	0.16	0.11	0.08	0.07
$\mathbf{y}_{o,j}$	$\mathbf{y}_{o,j} = \mathbf{x}_c + 0.3\mathbf{p}_1 \pm 0.1\mathbf{p}_2$				$\mathbf{y}_{o,j} = \mathbf{x}_c + 0.3\mathbf{p}_1 \pm 0.15\mathbf{p}_2$				
$\mathbf{y}_{e,j}$	$\mathbf{y}_{e,j} = \mathbf{x}_c - 0.3\mathbf{p}_1 \pm 0.2\mathbf{p}_2$				$\mathbf{y}_{e,j} = \mathbf{x}_c - 0.3\mathbf{p}_1 \pm 0.2\mathbf{p}_2$				

REFERENCES

[1] H. AMMARI, B. FITZPATRICK, H. KANG, M. RUIZ, S. YU, AND H. ZHANG, *Mathematical and Computational Methods in Photonics and Phononics*, Mathematical Surveys and Monographs, Vol. 235, Amer. Math. Soc., Rhode Island, 2018.

[2] H. AMMARI, B. FITZPATRICK, E. HILTUNEN, H. LEE, AND S. YU, *Honeycomb-lattice Minnaert bubbles*, SIAM J. Math. Anal., **52** (2020), 5441-5466.

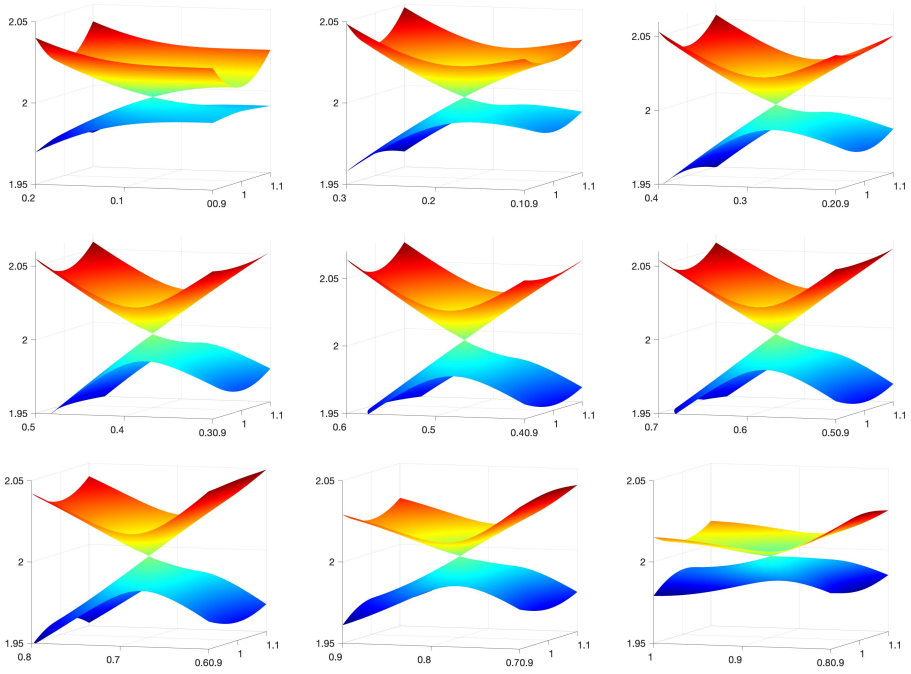

FIG. 5.2. *Dirac point at* $(\boldsymbol{\kappa}^*, \omega^*)$ *wherein* $\boldsymbol{\kappa}^* = (\pi, \kappa^*\pi) \in XM$ *and* $\kappa^* = 0.1, 0.2, \cdots, 0.9$*, and* $\omega^* = 2.0$*. The Dirac point is formed by the 2nd and 3rd band.*

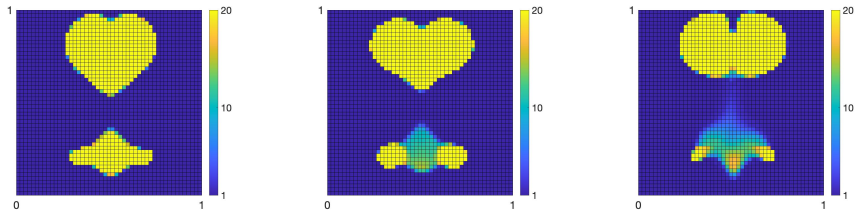

FIG. 5.3. *The dielectric function* $\rho(\mathbf{x})$ *that generates the Dirac point in Figure 5.2 for* $\kappa^* = 0.3, 0.6$*, and* 0.9*.*

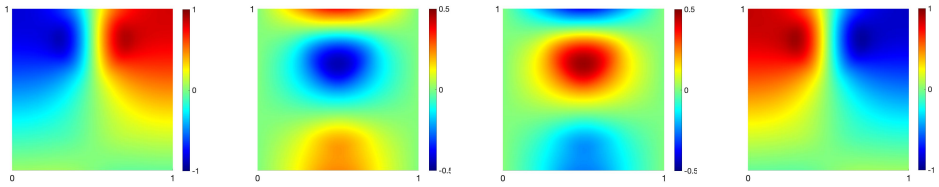

(a) (b) (c) (d)

FIG. 5.4. *The real part of the 2nd and 3rd Bloch mode* $\psi(\boldsymbol{\kappa}, \cdot)$ *with the optimized dielectric function* $\rho(\mathbf{x})$ *solved at* $\boldsymbol{\kappa}^* = (\pi, 0.3\pi)$*, which is plotted in Figure 5.3 (left). (a)(b):* $\boldsymbol{\kappa} = \boldsymbol{\kappa}^* - \frac{\pi}{100}\mathbf{p}_1$*; (c)(d):* $\boldsymbol{\kappa} = \boldsymbol{\kappa}^* + \frac{\pi}{100}\mathbf{p}_1$*. The parity of the Bloch modes* $\psi(\boldsymbol{\kappa}, \cdot)$ *swaps before and after crossing of the 2nd and 3rd spectral band at the Dirac point* $(\boldsymbol{\kappa}^*, \omega^*)$*.*

TABLE 5.2

The penalization parameter λ (second row), the minimum slope value μ^* for the Dirac cones (third row), and the dipole sources locations (fourth and fifth row) when $\boldsymbol{\kappa}^* = (\kappa^*\pi, 0)$.

κ^*	0.1	0.2	0.3	0.4	0.5	0.6	0.7	0.8	0.9
λ	1000	1000	2500	1000	2000	500	500	100	800
μ^*	0.02	0.11	0.10	0.26	0.34	0.38	0.40	0.37	0.2
$\mathbf{y}_{o,j}$	$\mathbf{y}_{o,j} = \mathbf{x}_c + 0.15\mathbf{p}_1 \pm 0.1\mathbf{p}_2$				$\mathbf{y}_{o,j} = \mathbf{x}_c + 0.15\mathbf{p}_1 \pm 0.1\mathbf{p}_2$				
$\mathbf{y}_{e,j}$	$\mathbf{y}_{e,j} = \mathbf{x}_c - 0.25\mathbf{p}_1 \pm 0.15\mathbf{p}_2$				$\mathbf{y}_{e,j} = \mathbf{x}_c - 0.15\mathbf{p}_1 \pm 0.15\mathbf{p}_2$				

TABLE 5.3

The penalization parameter λ (second row), the minimum slope value μ^* for the Dirac cones (third row), and the dipole sources locations (fourth and fifth row) when $\boldsymbol{\kappa}^* = (\kappa^*\pi, \kappa^*\pi)$.

κ^*	0.1	0.2	0.3	0.4	0.5	0.6	0.7	0.8	0.9
λ	2500	400	400	400	400	400	400	500	500
μ^*	0.15	0.70	0.39	0.35	0.48	0.44	0.40	0.38	0.53
$\mathbf{y}_{o,j}$	$\mathbf{y}_{o,1} = \mathbf{x}_c + 0.3\mathbf{p}_1 + 0.2\mathbf{p}_2$, $\mathbf{y}_{o,2} = \mathbf{x}_c + 0.3\mathbf{p}_1 - 0.2\mathbf{p}_2$								
$\mathbf{y}_{e,j}$	$\mathbf{y}_{e,1} = \mathbf{x}_c - 0.3\mathbf{p}_1 + 0.2\mathbf{p}_2$, $\mathbf{y}_{e,2} = \mathbf{x}_c - 0.3\mathbf{p}_1 - 0.2\mathbf{p}_2$								

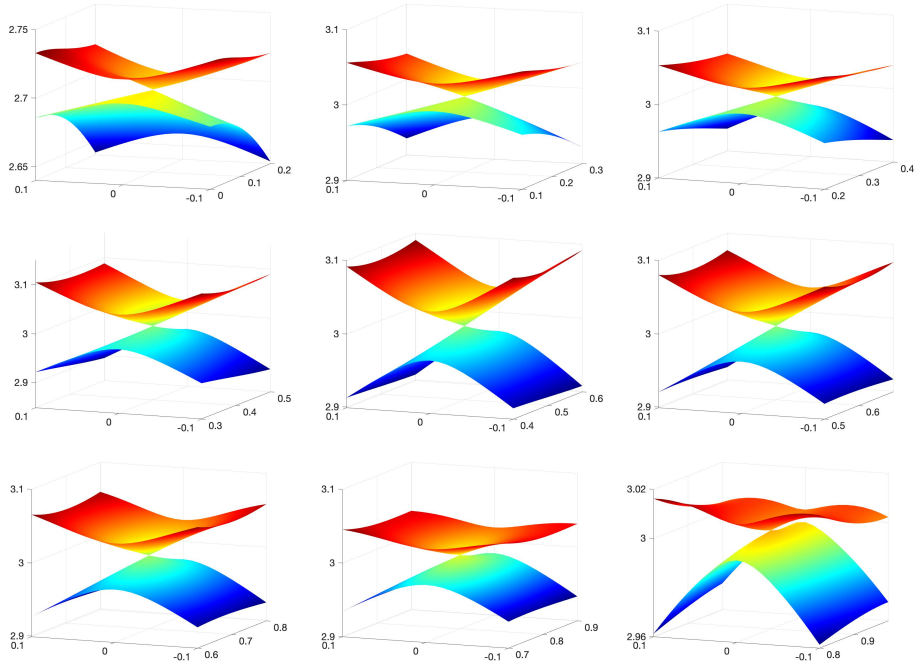

FIG. 5.5. *Dirac point at $(\boldsymbol{\kappa}^*, \omega^*)$ wherein $\boldsymbol{\kappa}^* = (\kappa^*\pi, 0) \in \Gamma X$ and $\kappa^* = 0.1, 0.2, \cdots, 0.9$. $\omega^* = 2.7$ for $\kappa^* = 0.1$ and $\omega^* = 3.0$ otherwise. The Dirac point is formed by the 3rd and 4th band.*

[3] H. AMMARI, H. KANG, AND H. LEE, *Layer Potential Techniques in Spectral Analysis*, Mathematical Surveys and Monographs, Vol. 153, Amer. Math. Soc., Rhode Island, 2009.

[4] G. BERKOLAIKO AND A. COMECH, *Symmetry and Dirac points in graphene spectrum*, J. Spectr. Theor., **8** (2018), 1099-1147.

[5] M. CASSIER AND M. WEINSTEIN, *High contrast elliptic operators in honeycomb structures*, Multiscale Model. & Sim., **19** (2021), 1784-1856.

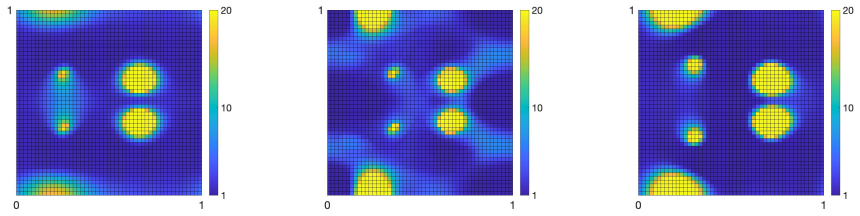

FIG. 5.6. *The dielectric function* $\rho(\mathbf{x})$ *that generates the Dirac point in Figure 5.5 for* $\kappa^* = 0.3, 0.6,$ *and* 0.9.

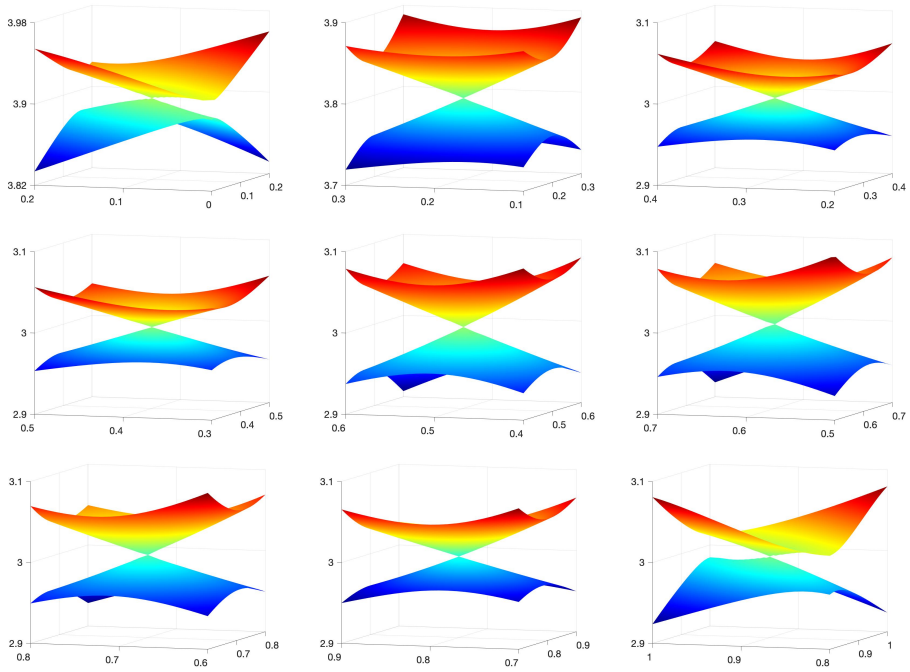

FIG. 5.7. *Dirac point at* $(\boldsymbol{\kappa}^*, \omega^*)$, *where* $\boldsymbol{\kappa}^* = (\kappa^*\pi, \kappa^*\pi) \in \Gamma M$ *with* $\kappa^* = 0.1, 0.2, \cdots, 0.9$. $\omega^* = 3.9$ *for* $\kappa^* = 0.1$, $\omega^* = 3.8$ *for* $\kappa^* = 0.2$, *and* $\omega^* = 3.0$ *otherwise. The Dirac point is formed by the 6th and 7th bands for* $\kappa^* = 0.1, 0.2$, *and by the 4th and 5th bands otherwise.*

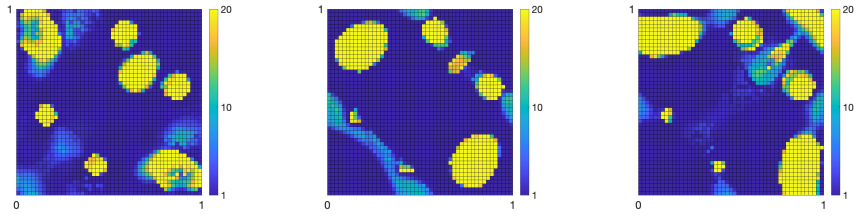

FIG. 5.8. *The dielectric function* $\rho(\mathbf{x})$ *that generates the Dirac point in Figure 5.7 for* $\kappa^* = 0.3, 0.6,$ *and* 0.9.

[6] A. Drouot and M. Weinstein, *Edge states and the valley Hall effect*, Adv. Math., **368** (2020): 107142.
[7] C. Fefferman and M. Weinstein, *Honeycomb lattice potentials and Dirac points*, J. Amer. Math. Soc., **25** (2012), 1169-1220.
[8] C. Fefferman, J. Lee-Thorp, and M. Weinstein, *Honeycomb Schrödinger operators in the strong binding regime*, Commun. Pur. Appl. Math., **6** (2018), 1178-1270.
[9] J. P. Lee-Thorp, M. I. Weinstein, and Y. Zhu, *Elliptic operators with honeycomb symmetry: Dirac Points, edge states and applications to photonic graphene*, Arch. Ration. Mech. An., **232** (2019), 1–63.
[10] V. Grushin, *Multiparameter perturbation theory of Fredholm operators applied to Bloch functions*, Math. Notes, **86** (2009), 767-774.
[11] F. Haldane and S. Raghu, *Possible realization of directional optical waveguides in photonic crystals with broken time-reversal symmetry*, Phys. Rev. Lett., **100** (2008), 013904.
[12] M. Z. Hasan and C. L. Kane, *Colloquium: topological insulators*, Rev Mod. Phys., **82** (2010): 3045-3067.
[13] G. Hsiao and W. L. Wendland, *Boundary Integral Equations*, Applied Mathematical Sciences, Vol. 164, Springer Berlin Heidelberg, 2008.
[14] R. Keller, J. Marzuola, B. Osting, and M. Weinstein, *Spectral band degeneracies of $\frac{\pi}{2}$-rotationally invariant periodic Schrödinger operators*, Multiscale Modeling & Simulation, **16** (2018), 1684-1731.
[15] A. Khanikaev, et al., *Photonic topological insulators*, Nat. Mater., **12** (2013), 233-239.
[16] R. Kress, *Linear Integral Equations* (3rd edition), Applied Mathematical Sciences, Vol. 82, Springer.
[17] P. Kuchment and O. Post, *On the spectra of carbon nano-structures*, Comm. Math. Phys., **275** (2007), 805-826.
[18] M. Lee, *Dirac cones for point scatterers on a honeycomb lattice*, SIAM J. Math. Anal., **48** (2016), 1459–1488.
[19] X. Liang and S. Johnson, *Formulation for scalable optimization of microcavities via the frequency-averaged local density of states*, Opt. Express, **21** (2013), 30812–30841.
[20] J. Lin and H. Zhang, *Mathematical theory for topological photonic materials in one dimension*, J. Phys. A: Math. Theor., **55** (2022): 495203.
[21] W. Li, J. Lin, J. Qiu, and H. Zhang, *Interface Modes in Honeycomb Topological Photonic Structures with Broken Reflection Symmetry*, 2024, arXiv:2405.03238.
[22] W. Li, J. Lin, and H. Zhang, *Dirac points for the honeycomb lattice with impenetrable obstacles*, SIAM J. Appl. Math., **83** (2023): 1546-1571.
[23] L. Lu, J. Joannopoulos, and Marin Soljacic, *Topological photonics*, Nat. Photonics, **8** (2014), 821-829.
[24] T. Ma and G. Shvets, *All-Si valley-Hall photonic topological insulator*, New J. Phys., **18** (2016), 025012.
[25] M. Makwana, R. Craster, and S. Guenneau, *Topological beam-splitting in photonic crystals*, Opt. Express, **27** (2019), 16088-16102.
[26] T. Ochiai and M. Onoda, *Photonic analog of graphene model and its extension: Dirac cone, symmetry, and edge states*, Phys. Rev. B, **80** (2009), 155103.
[27] T. Ozawa, et al. *Topological photonics*, Rev. Mod. Phys., **91** (2019), 015006.
[28] S. Raghu and F. D. M. Haldane, *Analogs of quantum-Hall-effect edge states in photonic crystals*, Phys. Rev. A, **78** (2008), 033834.
[29] M. Rechtsman, et al., *Photonic Floquet topological insulators*, Nature, **496** (2013), 196-200.
[30] J. C. Slonczewski and P. R. Weiss, *Band structure of graphite*, Phys. Rev., **109** (1958), 272-279.
[31] D. Torrent and J. Sánchez-Dehesa, *Acoustic analogue of graphene: observation of Dirac cones in acoustic surface waves*, Phys. Rev. Lett., **108** (2012), 174301.
[32] P. Wallace, *The band theory of graphite*, Phys. Rev., **71** (1947), 622–634.
[33] L. Wu and X. Hu, *Scheme for achieving a topological photonic crystal by using dielectric material*, Phys. Rev. Lett., **114** (2015), 223901.
[34] Z. Yang, et al. *Topological acoustics*, Phys. Rev. Lett., **114** (2015), 114301.
[35] R. Brayton, S. Director, G. Hachtel and L. Vidigal, *A new algorithm for statistical circuit design based on quasi-newton methods and function splitting*, IEEE Transactions on Circuits and Systems, **26** (1979), 784-794.